UNITED NATIONS EDUCATIONAL, SCIENTIFIC AND CULTURAL ORGANIZATION
INTERNATIONAL ATOMIC ENERGY AGENCY
INTERNATIONAL CENTRE FOR THEORETICAL PHYSICS
I.C.T.P., P.O. BOX 586, 34100 TRIESTE, ITALY, CABLE: CENTRATOM TRIESTE

H4.SMR/916 -14

SEVENTH COLLEGE ON BIOPHYSICS:

Structure and Function of Biopolymers: Experimental and Theoretical Techniques.

4 - 29 March 1996

Biological Microcalorimetry - II

Pedro L. MATEO
Department of Physical Chemistry
University of Granada
18071 Granada
SPAIN

Strategies for the Investigation & Alteration of Protein Stability

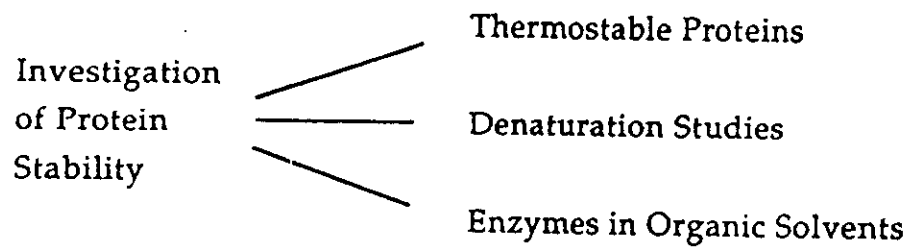

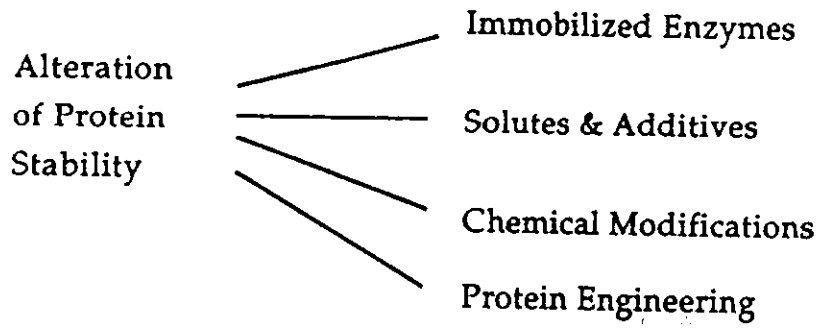

A. Deriu et al. Biophys. Chem. 53 145 (1994)

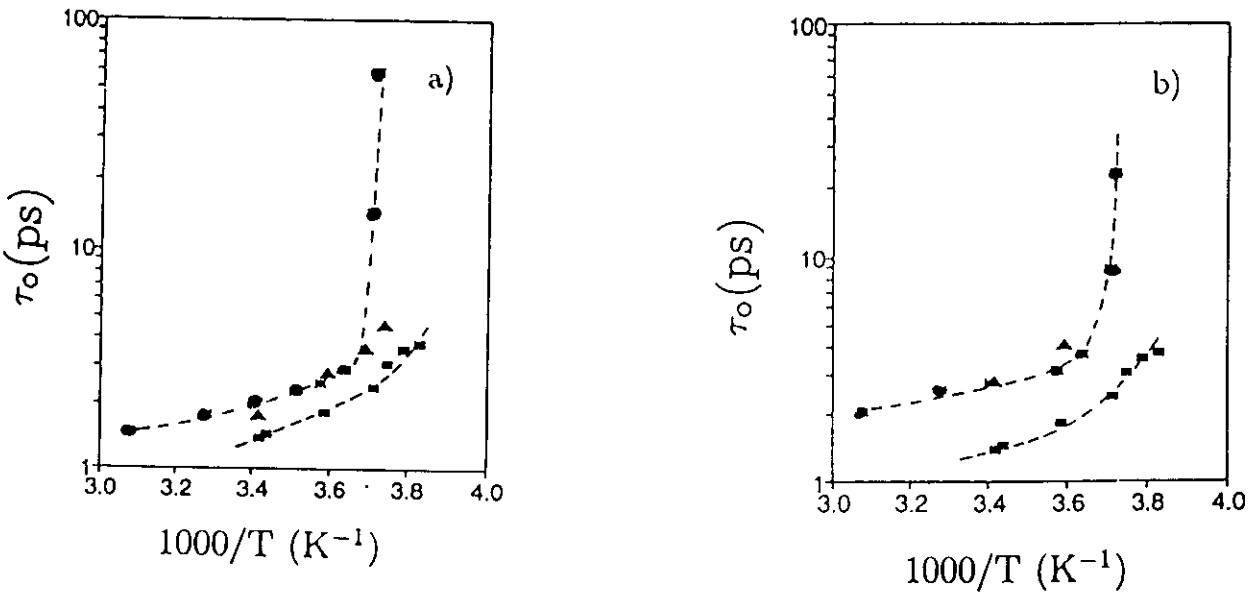

Fig. 4. Arrhenius plot of residence times τ_0 for pure H_2O (■), hyaluronic acid (▲) and agarose gel water (●). Gel concentrations are 1% (a) and 8% (b).

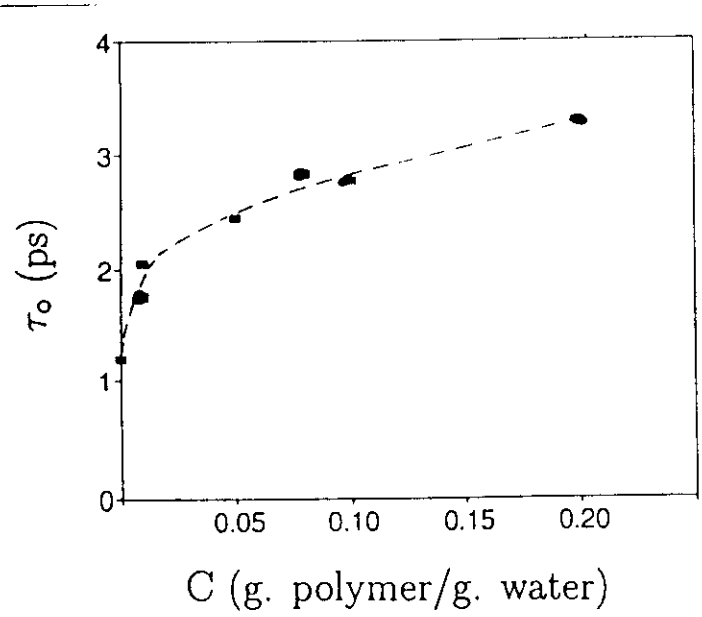

Fig. 5. Dependence on concentration C of residence times τ_0 for agarose (■) and HA (■) gel water at $T = 293$ K.

A. Derici et al. Biophys. Chem. 53, 145 (1994)

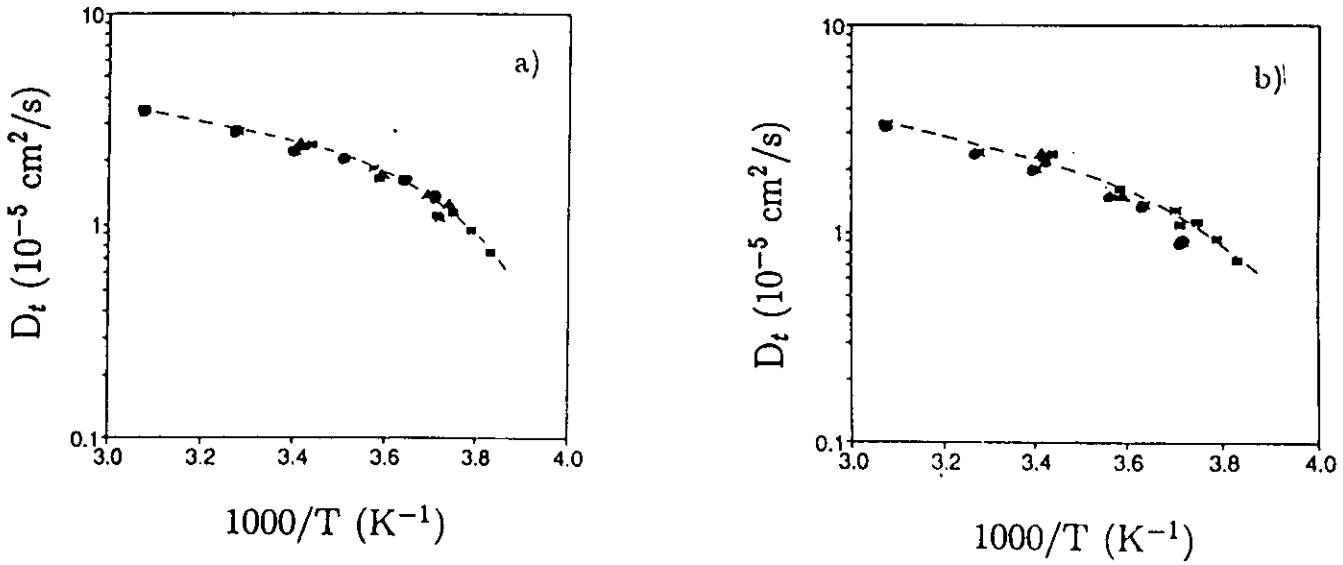

Fig. 6. Arrhenius plot of translational diffusion coefficients D_t for pure H_2O (■), hyaluronic acid (▲) and agarose gels (●). Gel concentrations are 1% (a) and 8% (b).

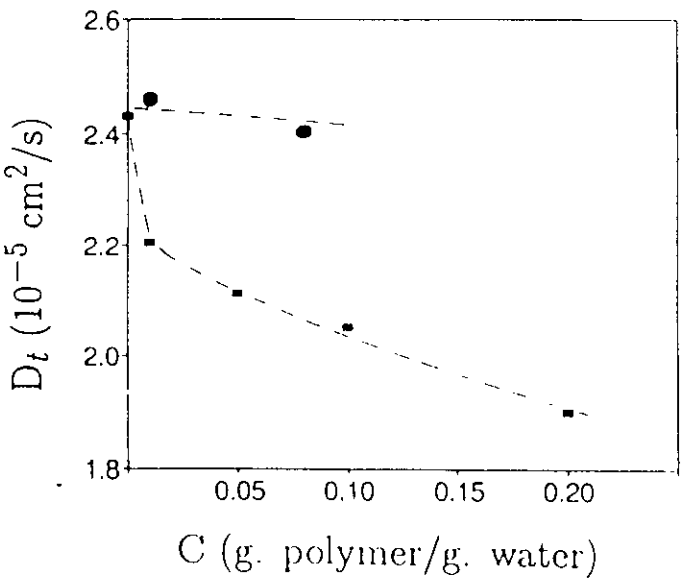

Fig. 7. Dependence on concentration C of translational diffusion coefficients D_t for agarose (■) and HA (■) gel water at $T = 293$ K.

Diffusivity parameter for water in agarose gels.

- A. Denis et al, Europhys Lett. 24, 351 (1993)
- A. Denis et al, Biophys chem. 53, 145 (1994)

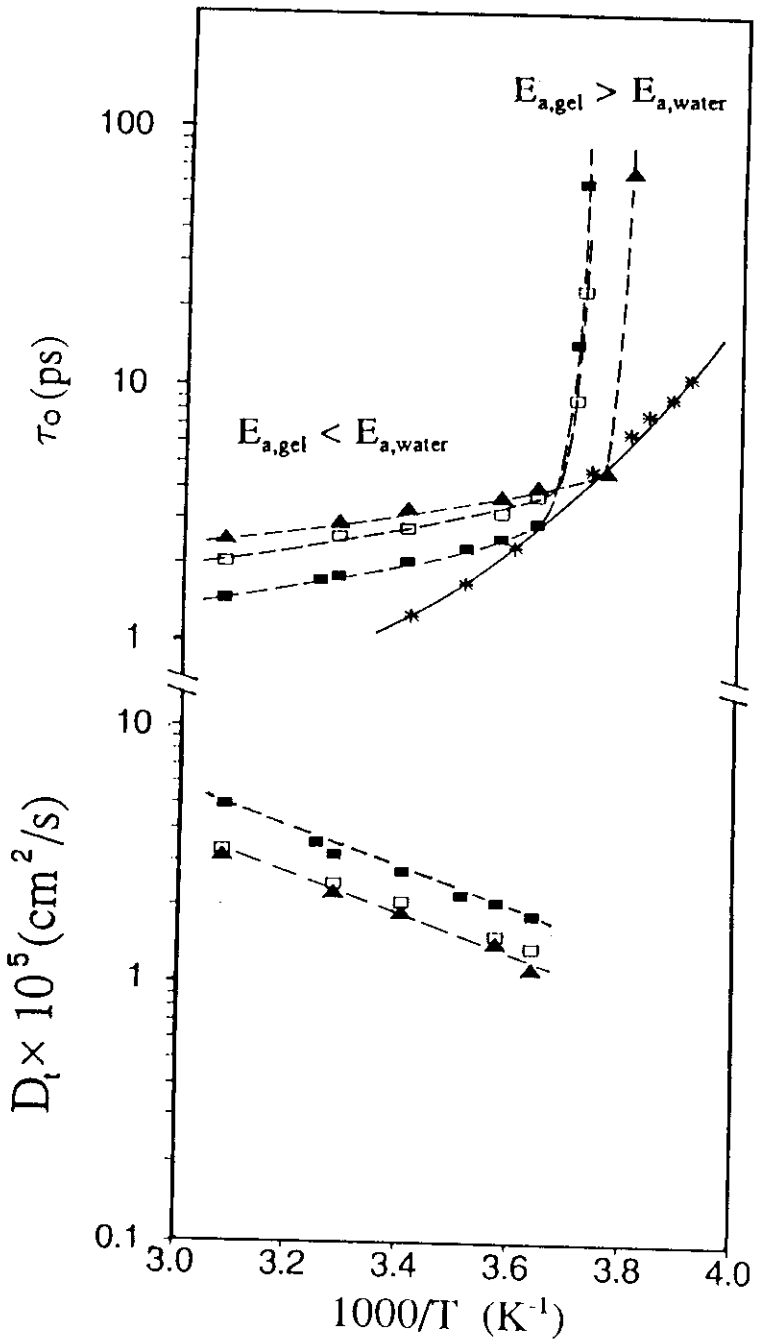

Gel concentration C
(C = g polymer / g. water)

▲ C = 0.01
□ C = 0.10
■ C = 0.20

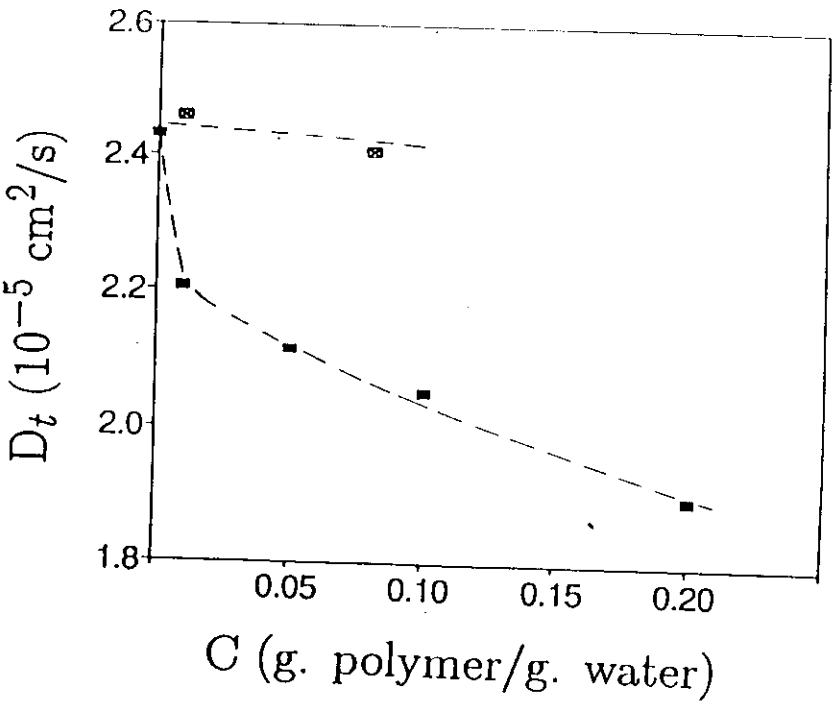

■ Agarose gel.

⊠ Hyaluronate gel.

Lineshape deconvolution.

$$S(Q,\omega) = f^{I} W^{I} \delta(\omega) + f^{II} W^{II} S_{rot}(Q,\omega) + f^{III} W^{III} \cdot \left[S_{trans}(Q,\omega) \otimes S_{rot}(Q,\omega) \right]$$

$$S_{trans} = \frac{\Gamma(Q)}{\Gamma^2(Q) + \hbar\omega^2} \quad \Rightarrow \quad \Gamma(Q) = \frac{DQ^2}{1 + D\tau_0 Q^2}$$

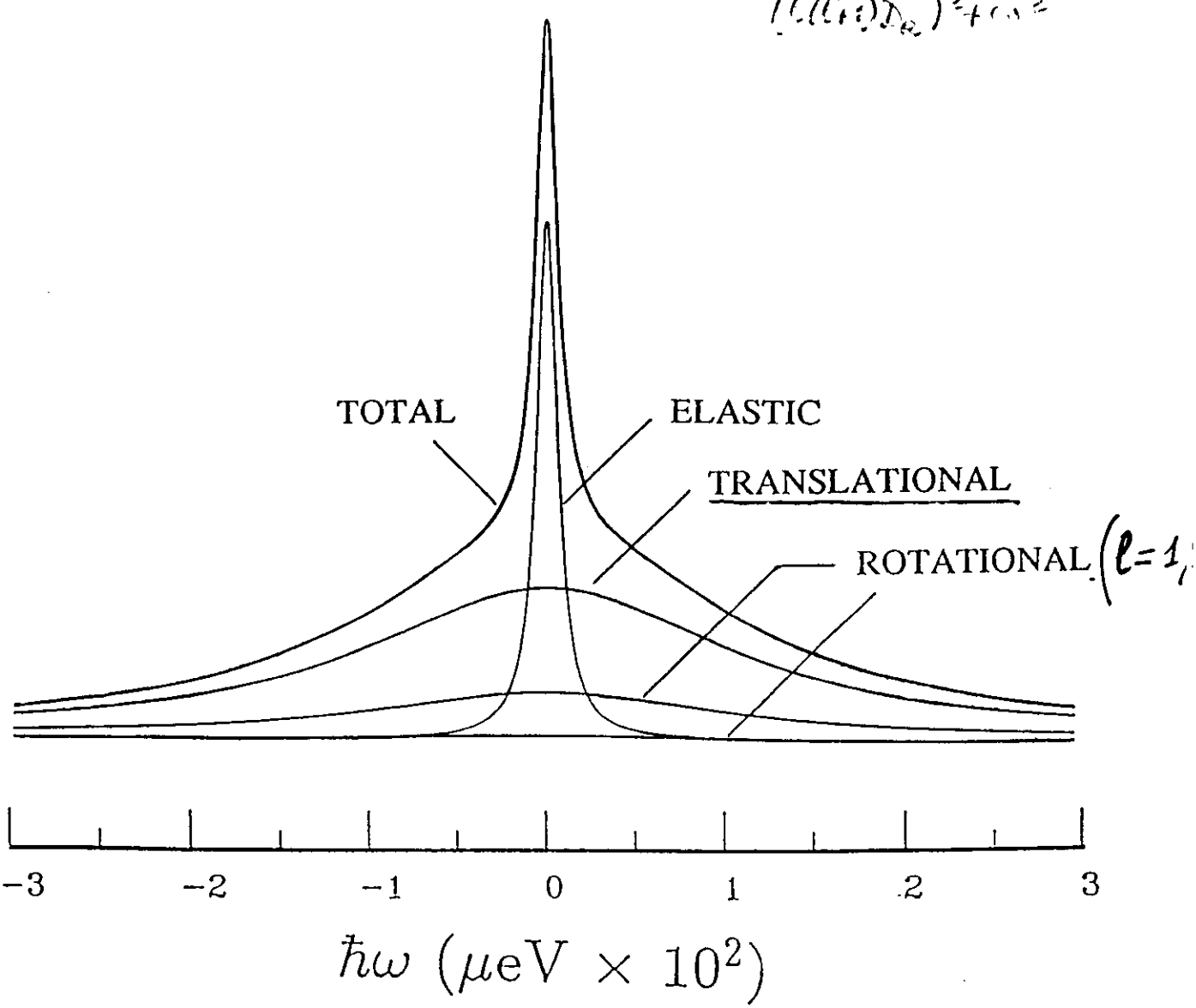

Hierarchy of structure in an agarose gel

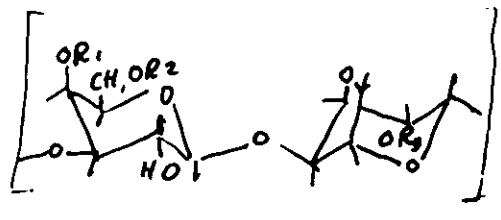

$R_1 = R_2 = R_3 = H$ ⇒ native agarose

Heat ↑ | ↓ Cool

time.

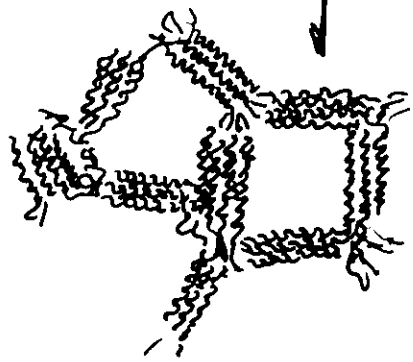

DPPC $L_\beta \rightarrow L_\alpha$ transition

S. König, W. Pfeiffer, T. Bayerl, D. Richter, E. Sackmann - J. Phys. (France) In Press.

IN5 →

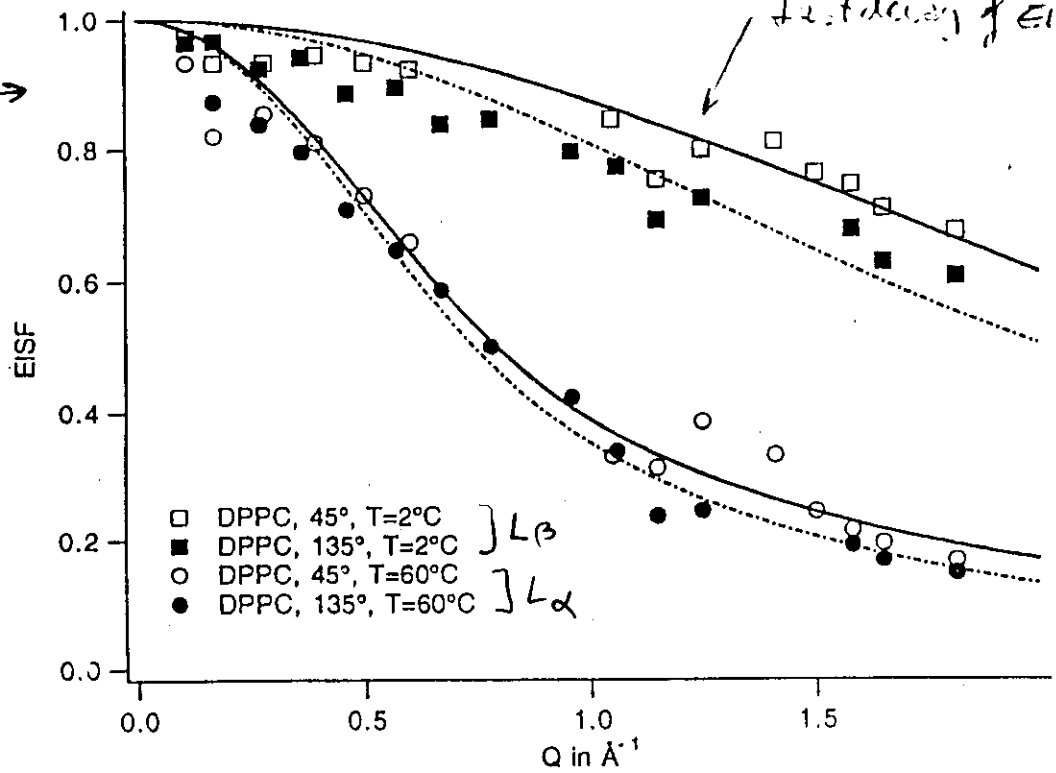

fast decay of EISF even at 2°C

} isotropic motion

IN10 →

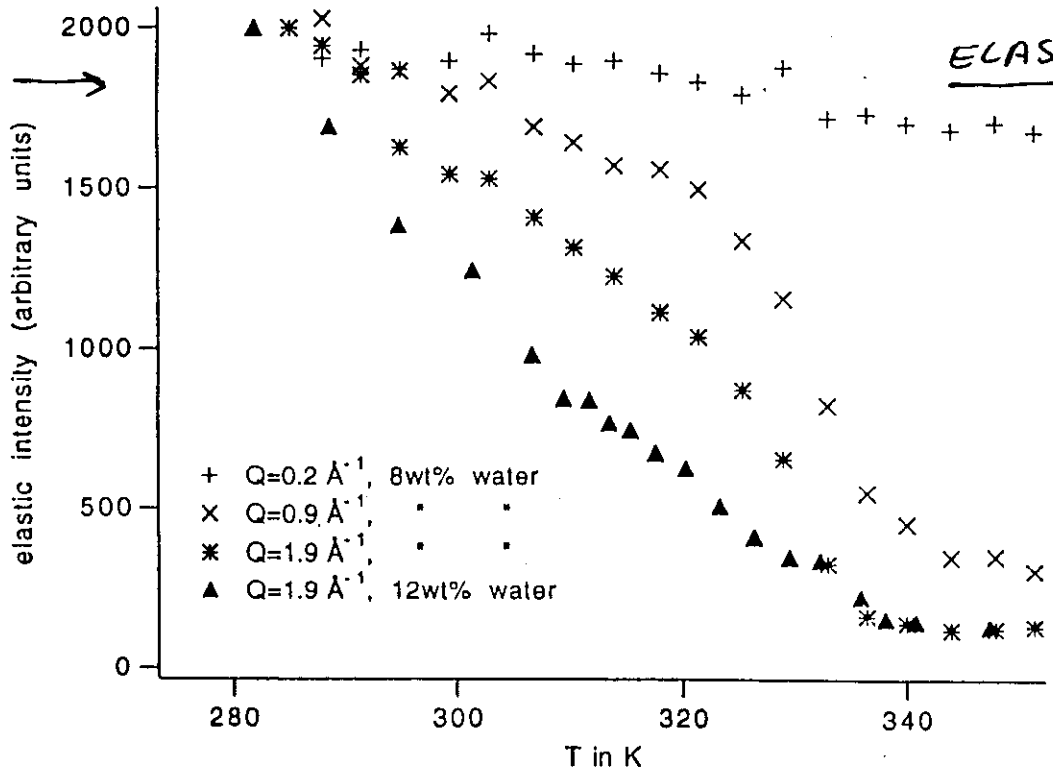

ELASTIC INTENSITY

$L\beta \rightarrow L\alpha$ transition

- Increase in slope in going towards medium scattering vectors (mobility determined by motion of small amplitude defects)

Dipalmitoylphosphatidylcholine (DPPC)

- Protonated and deuterated lipids
- IN5 + IN10 + NESSIE

EISF

IN5 →

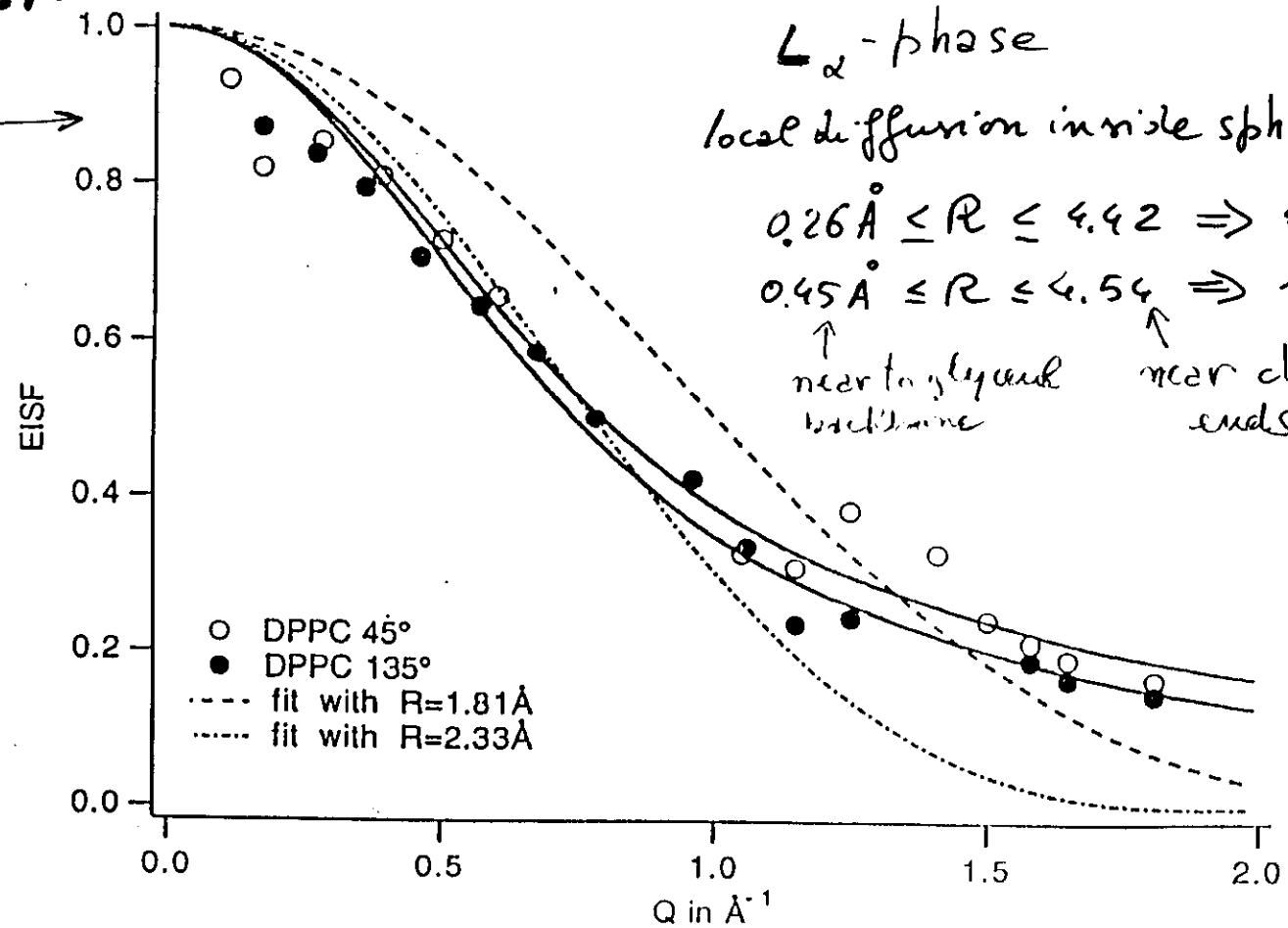

L_α - phase

local diffusion inside spheres

$0.26\,Å \leq R \leq 4.42 \Rightarrow 45°$

$0.45\,Å \leq R \leq 4.54 \Rightarrow 135°$

↑ near to glycerol backbone

↑ near chain ends

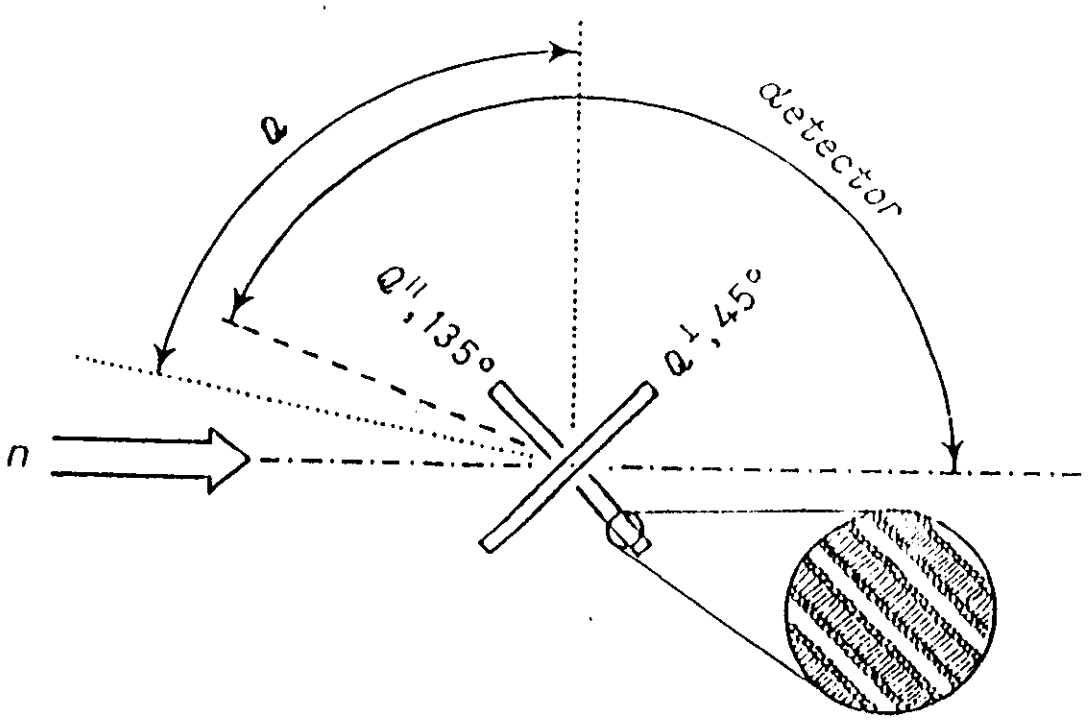

Motional processes in lipid bilayers

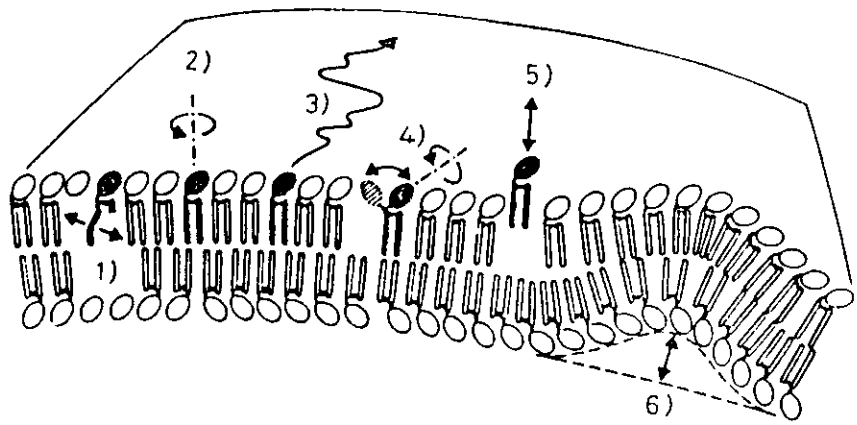

1 - Chain defect motions (analogous to γ - processes in polymers)

2 - Rotational diffusion of the lipid molecule

3 - In-plane lateral diffusion of the lipid molecule

4 - rotational and flip-flop motion of head groups

5 - vertical vibrational motions of the lipid

6 - Collective undulations of the whole bilayer.

SOD

{ C. Andreani, A. Filabozzi - [- Biophys J. 68, 2319 (1995)
A. Desideri - [- Physica B, (1996) - In press
A. Deriu, D. Di Cola

■ D_2O-hydrated myoglobin
(from W. Doster et al, Nature 337, 754 (1989)

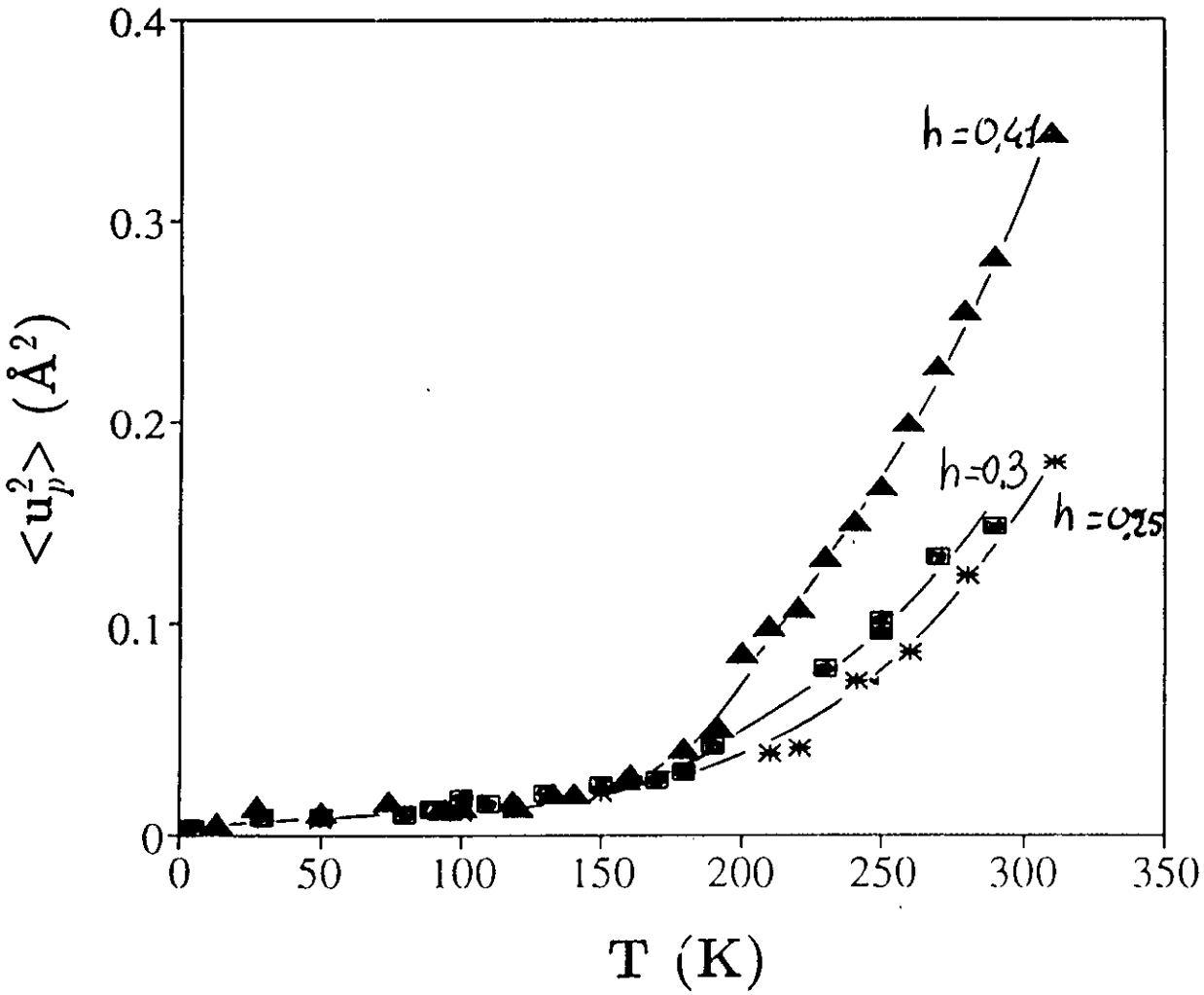

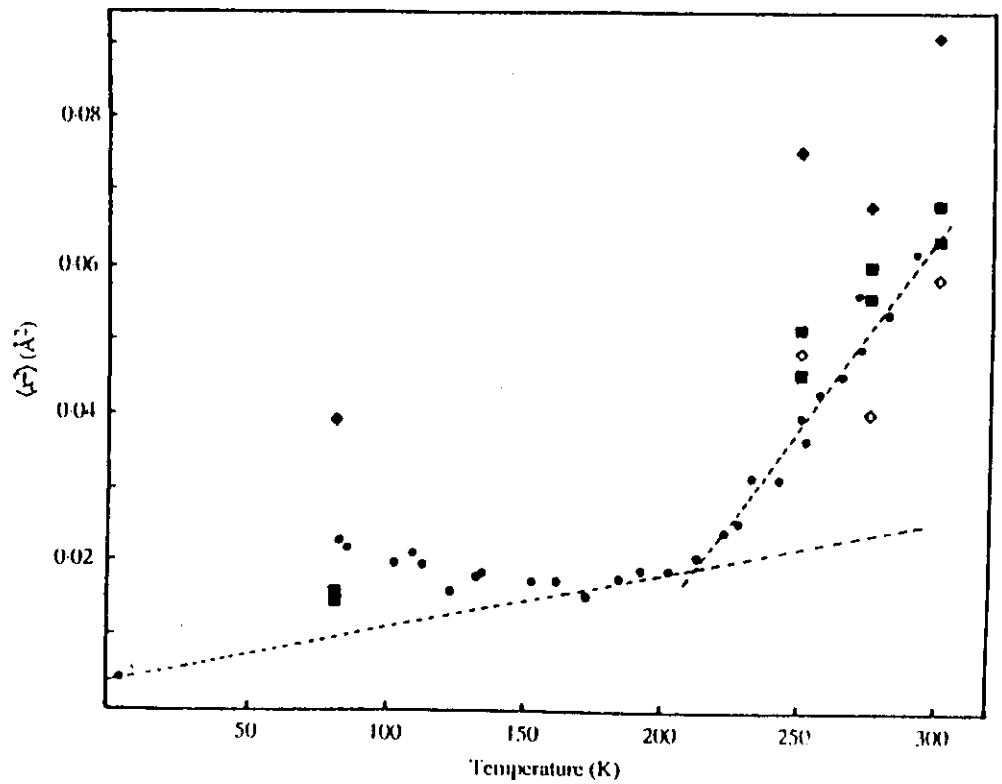

- Mössbauer-iron
- X-ray - iron
- X-ray - His 9
- X-ray - His 6

J. Smith et al. Proc. Natl. Acad. Sci. U.S.A. 87 (1990) 1601

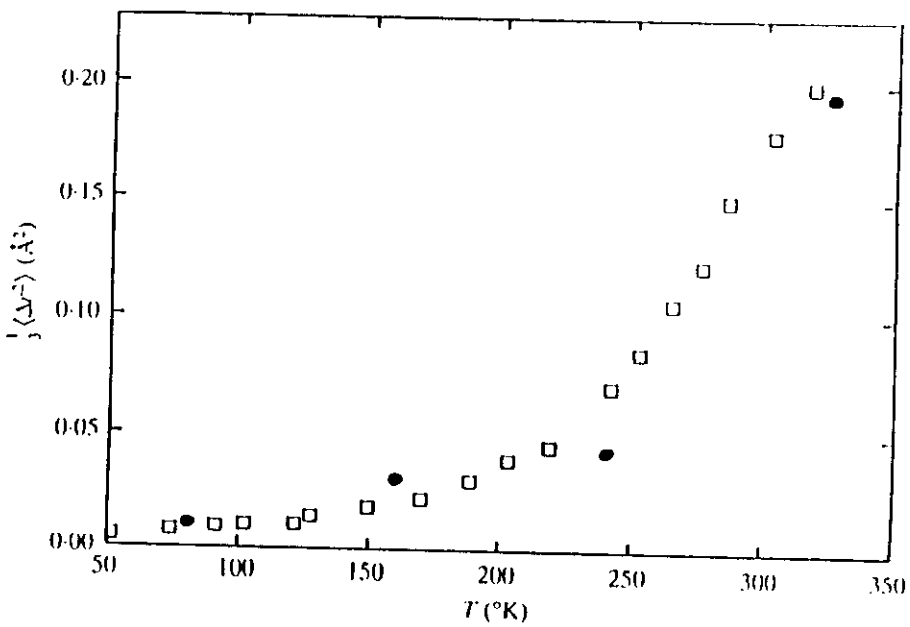

- M.D simulation

W. Doster, S. Cusack, W. Petry, Nature 337 (1989) 754

IN13

$I_{el}(Q) = S(Q, \omega \simeq 0)$

$\Delta E \simeq 10\ \mu eV$ (FWHM)

$\lambda_0 = 2.23\ \text{Å}$

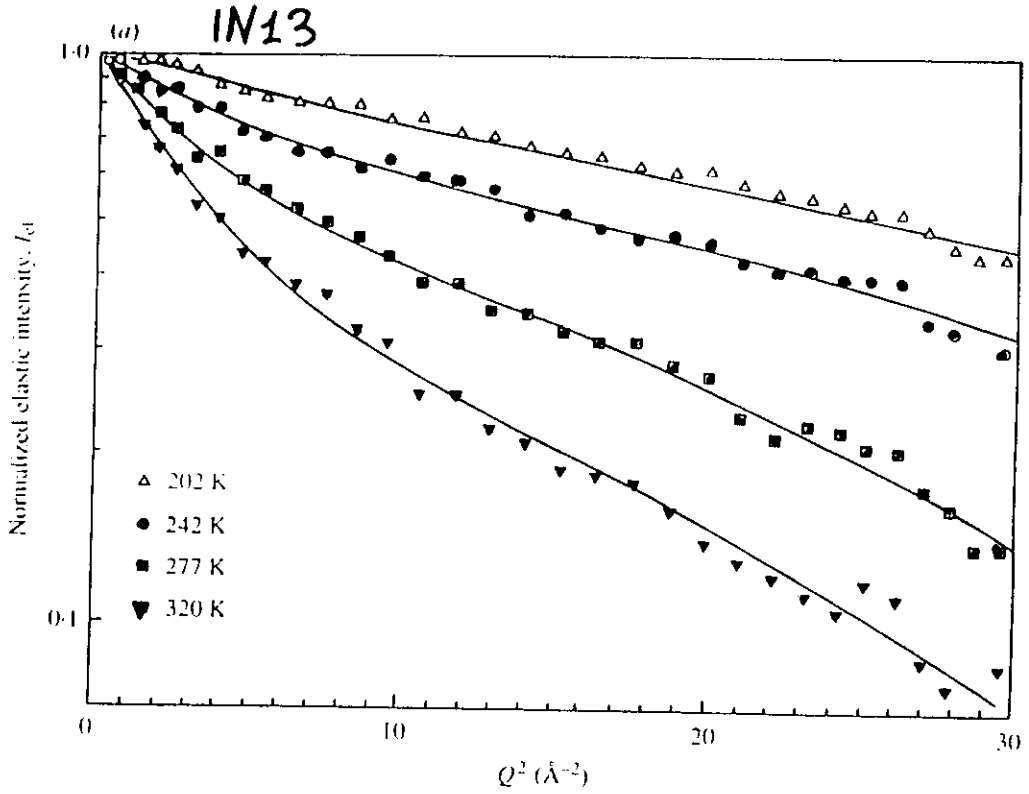

MD simulation

$S(Q,0) = \sum_i b_i^2 e^{-Q^2 \langle R_i^2 \rangle}$

(---) initial slope: ($Q^2 \to 0$)

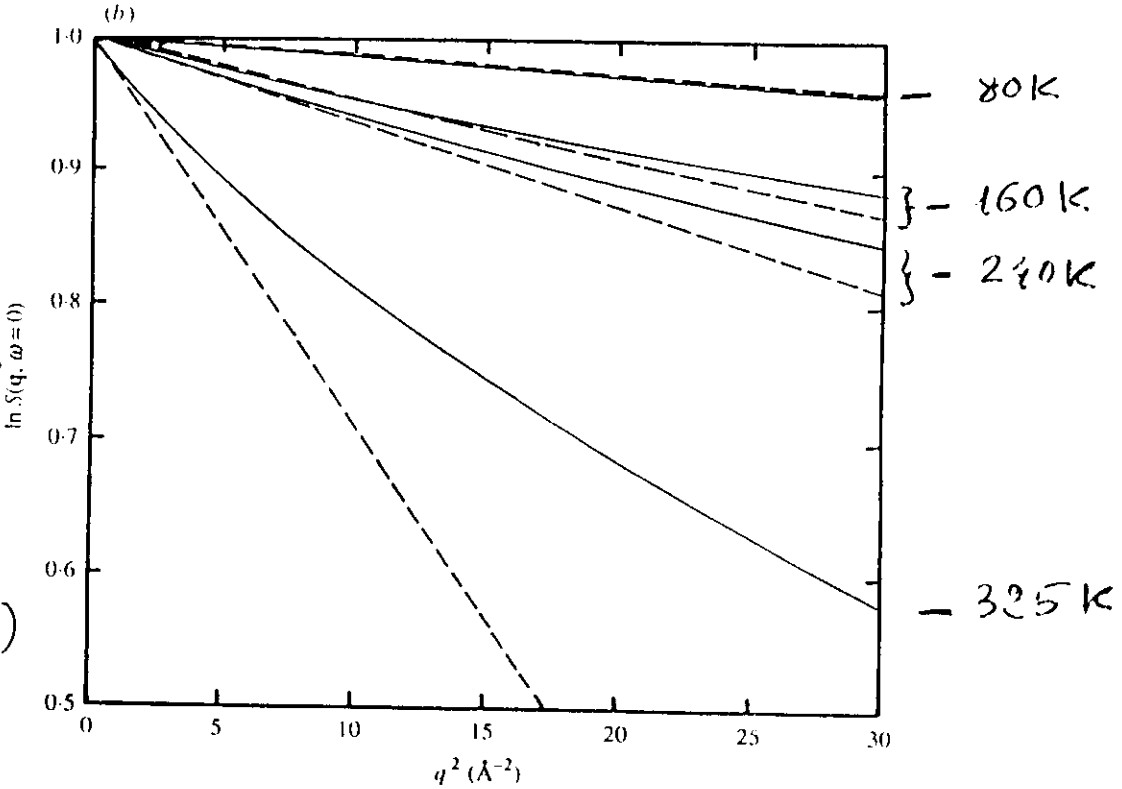

D_2O-hydrated myoglobin (0.38 g D_2O per g protein)

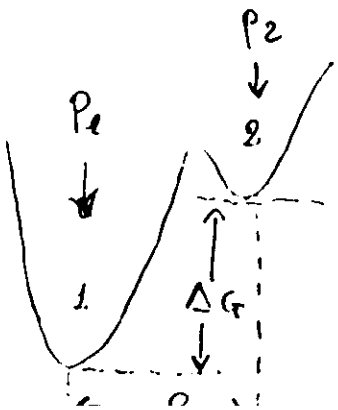

$$S(Q,0) = e^{-Q^2 \langle R^2 \rangle_G} \left\{ 1 + 2 P_1 P_2 \left[1 - \frac{\sin(Qd)}{Qd} \right] \right.$$

$$\langle R^2 \rangle = \langle R^2 \rangle_G + \frac{P_1 P_2 d^2}{3}$$

$$d = 1.5\ \text{Å}$$

N. Doster, S. Cusack, W. Petry, PRL 65 (1990) 1080

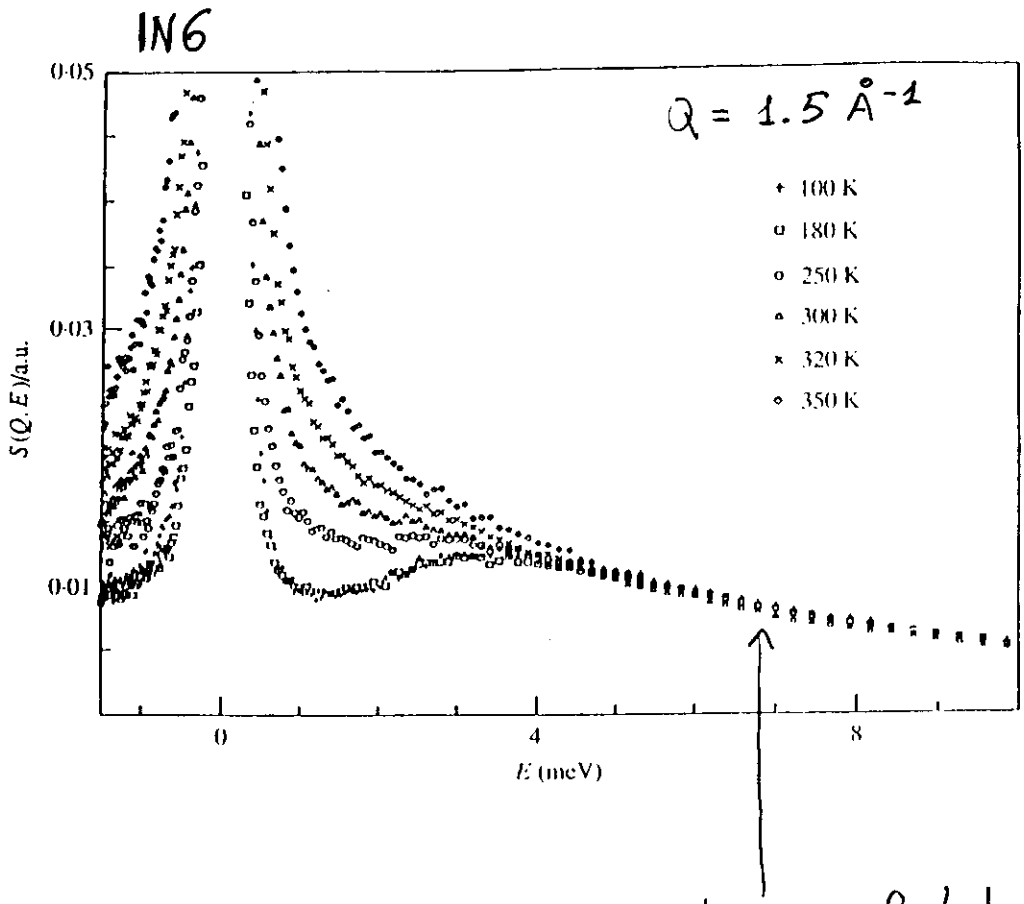

Data rescaled by He Bose factor to a common temperature (180K)

D_2O-exchanged myoglobin.

S. Cusack, W. Doster, Biophys. J. 58 (1990) 243

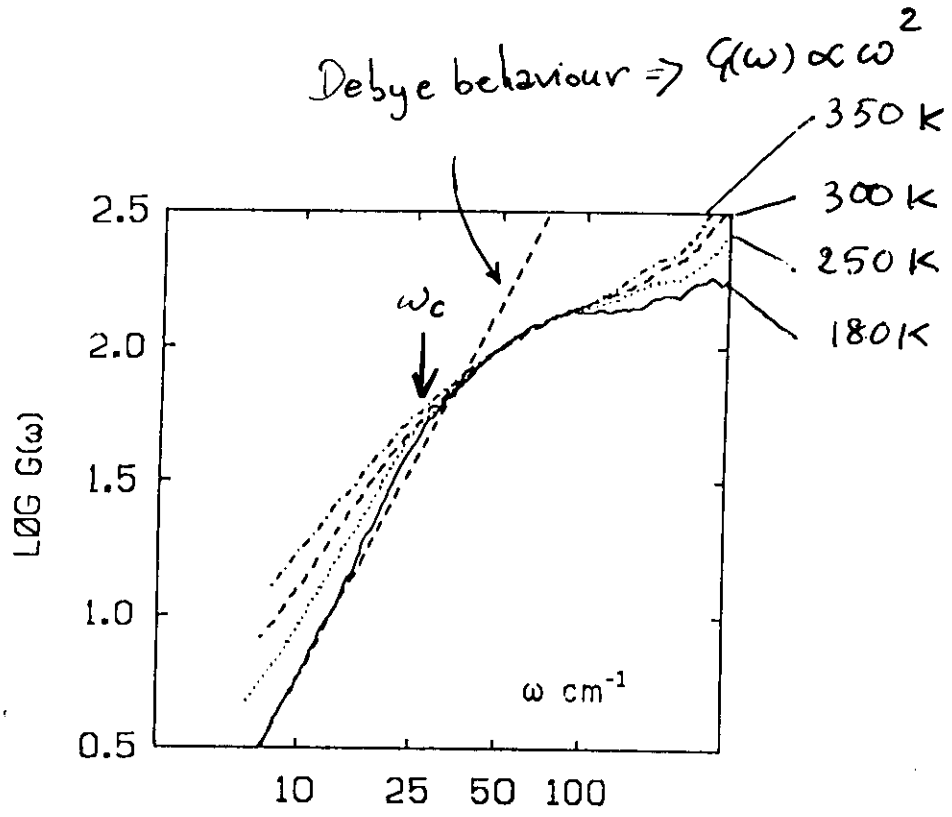

$$G(\omega) = \lim_{Q\to 0} \frac{\hbar\omega}{\hbar Q^2}\left(e^{\frac{\hbar\omega}{k_B T}} - 1\right) S_{inc}(Q,\omega) =$$

$$= \sum_{1}^{3N-6}{}_{\lambda} \sum_{1}^{N}{}_{\alpha} \frac{\sigma_\alpha^{inc}}{4\pi m_\alpha} |\mathbf{c}_\alpha^\lambda|^2 \delta(\omega - \omega_\lambda)$$

$\omega < \omega_c \Rightarrow$ Debye behaviour $\quad G(\omega) \propto \omega^2$

$\omega > \omega_c \Rightarrow$ Fractal behaviour $\quad G(\omega) \propto \omega^{d-1}$

$\omega_c \simeq 25$ cm^{-1} ; $v_s \simeq 3{,}000$ m/s $\quad \xi \simeq 40$ Å

S. Cusack & W. Doster, Biophys. J 58 (1990) 243

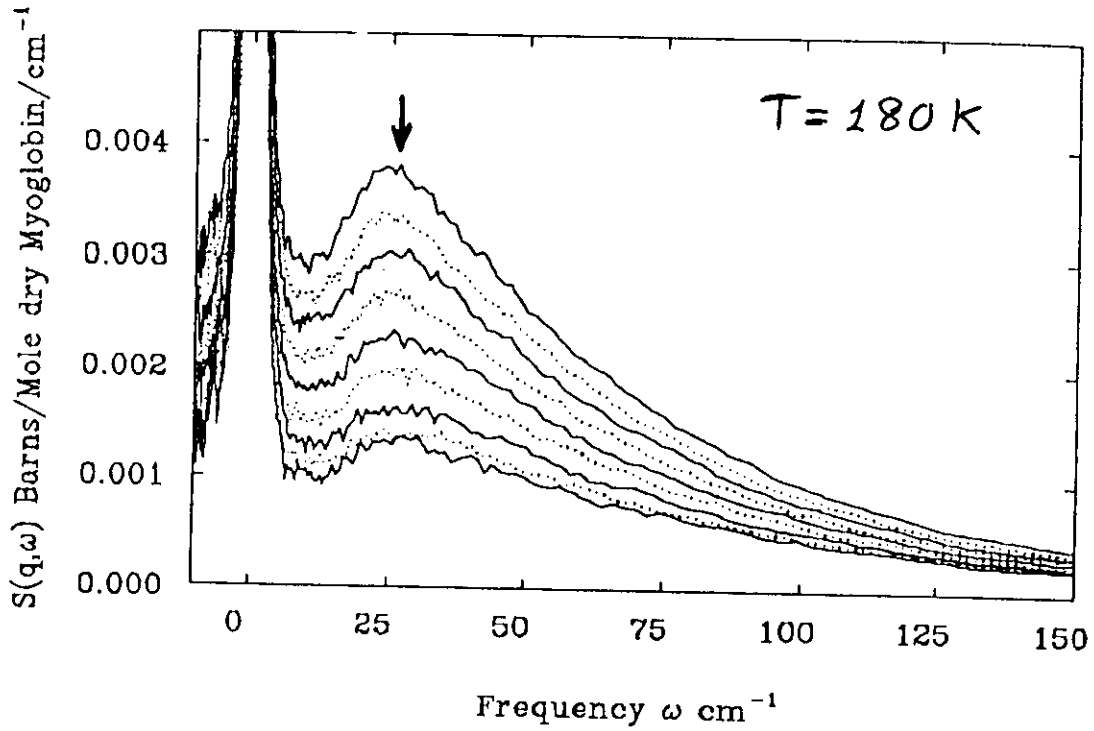

Scattering angles

111.6°
97.3°
84.6°
71.8°
61.2°
50.6°
35.4°
25.9°

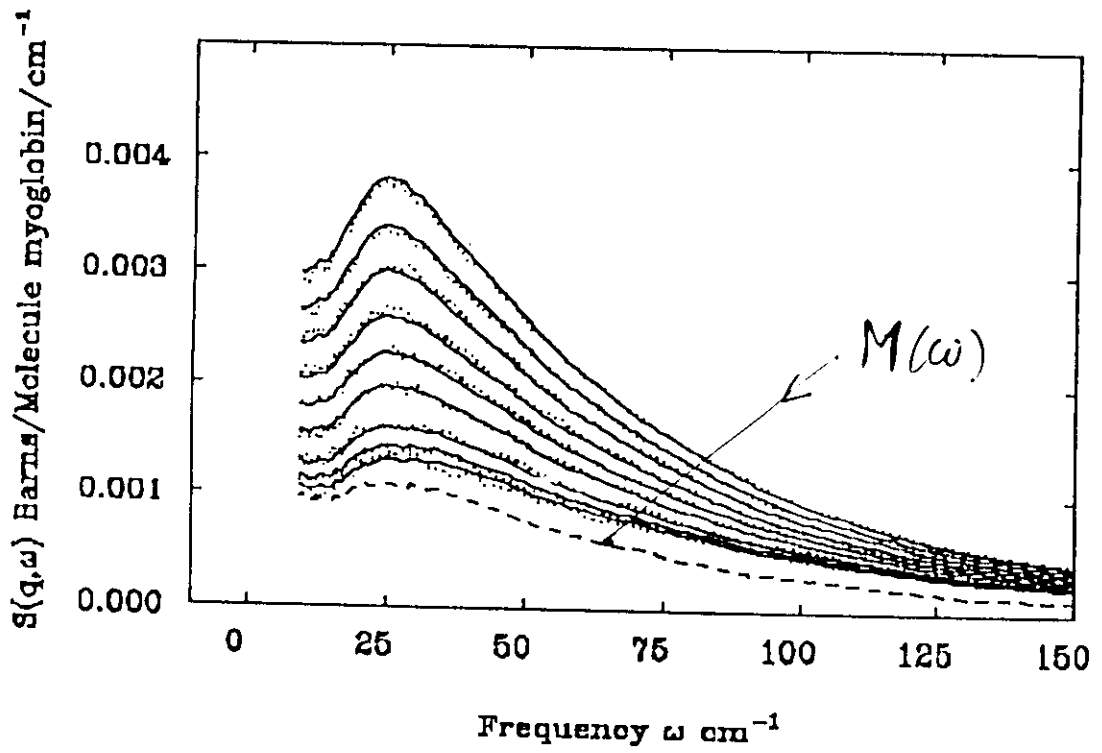

D_2O-hydrated myoglobin at 180 K

$$S(Q,\omega) = \frac{\hbar Q^2}{6\omega} \frac{1}{(e^{\hbar\omega/k_BT} - 1)} G(\omega)\, e^{-Q^2 U^2_{vib}} + M(\omega)$$

Differential Scanning Calorimetric Study of the Thermal Unfolding of Myosin Rod, Light Meromyosin, and Subfragment 2

JOSE L. LOPEZ-LACOMBA, M. GUZMAN, MANUEL CORTIJO,* PEDRO L. MATEO, *Departmento de Quimica Fisica, Facultad de Ciencias, Universidad de Granada, 18071 Granada, Spain;* RAUL AGUIRRE,† STEPHEN C. HARVEY, and HERBERT C. CHEUNG,‡ *Department of Biochemistry, University of Alabama at Birmingham, Birmingham, Alabama 35294*

Synopsis

The thermal unfolding of myosin rod, light meromyosin (LMM), and myosin subfragment 2 (S-2) was studied by differential scanning calorimetry (DSC) over the pH range of 6.5–9.0 in 0.5*M* KCl and either 0.20*M* sodium phosphate or 0.15*M* sodium pyrophosphate. Two rod samples were examined: one was purified by Sephadex G-200 without prior denaturation (native rod), and the other was purified by a cycle of denaturation–renaturation followed by Sephacryl S-200 chromatography (renatured rod). There were clearly distinguishable differences in the calorimetric behavior of these two samples. At pH 7.0 in phosphate the DSC curves of native rod were deconvoluted into six endothermic two-state transitions with melting temperatures in the range of 46–67°C and a total enthalpy of 4346 kJ/mol. Under identical conditions the melting profile of LMM was resolved into five endothermic peaks with transition temperatures in the range of 45–66°C, and the thermal profile of long S-2 was resolved into two endotherms, 46 and 57°C. Transition 4 observed with native rod was present in the deconvoluted DSC curve for long S-2, but absent in the DSC curve for LMM. This transition was identified with the high-temperature transition detected with long S-2 and attributed to the melting of the coiled-coil α-helical segment of subfragment 2 (short S-2). The low-temperature transition of long S-2 was attributed to the unfolding of the hinge region. The smallest transition temperatures observed for all three fragments were 45–46°C. It is suggested that the most unstable domain in rod (domain 1) responsible for the 46°C transition includes both the hinge region, which is the C-terminal segment of long S-2, and a short N-terminal segment of LMM. This domain, accounting for 21% of the rod structure, contains the S-2/LMM junction, and upon proteolytic cleavage yields the C-terminal and N-terminal ends of long S-2 and LMM, respectively. Over the pH range of 6.5–7.5, the observed specific heat of denaturation of rod was approximately equal to the sum of the specific heats of LMM and S-2. This finding provides an additional argument for the existence of independent domains in myosin rod.

INTRODUCTION

Energy transduction is a fundamental phenomenon in biological processes. In muscle this phenomenon relates to the conversion of Gibbs energy released from the hydrolysis of ATP by myosin heads (subfragment 1) to mechanical

*Present address: Departamento de Quimica Fisica Farmaceutica, Facultad de Farmacia, Universidad Complutense, 28071 Madrid, Spain.

†Present address: Department of Biochemistry, University of Chile, Santiago, Chile.

‡To whom correspondence should be addressed.

Biopolymers, Vol. 28, 2143–2159 (1989)

CCC 0006-3525/89/122143-17$04.00

work (force generation). Current models of contraction postulate two hinge regions in the myosin molecule. In the sliding filament model, one hinge is located between subfragment 1 (S-1) and the coiled-coil α-helical rod, allowing the myosin heads to rotate during contraction,[1,2] and a second hinge is located within the rod portion of the molecule, facilitating cyclic attachment and detachment of the heads to the actin filament. In the helix-coil model,[3,4] the second hinge is thought to be the site of energy transduction at which force is generated.

Considerable efforts have been directed toward detecting the putative hinge regions and identifying their locations. The existence of a hinge between S-1 and rod has been demonstrated in solution and in assembled filamentous structure by a variety of techniques (see reviews by Harvey and Cheung[5] and Harrington and Rodgers[6]). The question of flexibility within the rod remains unsettled.[5] Several early studies have been published that were interpreted as indicating a flexible hinge within myosin rod. The work of Burke et al.,[7] on the basis of proteolytic digestion, thermal denaturation, and viscosity, indicated that myosin rod contained a segment of relatively low thermal stability flanked by two domains of higher stability, thus suggesting a flexible hinge in the rod. Highsmith et al.[8] used transient electric birefringence to investigate myosin rod, subfragment 2 (S-2), and light meromyosin (LMM), and concluded that myosin rod was flexible within the S-2 segment. This finding was corroborated by a subsequent study in which depolarized light scattering and proton nmr were used to investigate the flexibility problem.[9] More recently, Rodgers and Harrington[10] reexamined the question of rod flexibility by using quasi-elastic light scattering and optical rotation to measure the radius of gyration and helical content of rod, LMM, and S-2, and interpreted the results in terms of hinging of myosin rod within the LMM/S-2 junction between 20 and 40°C. In spite of these and other studies, several reports support the notion that myosin rod is relatively stiff and has only a limited degree of flexibility (see Harvey and Cheung[5]). Fluorescence depolarization studies by Harvey and Cheung[11] showed no detectable flexibility at neutral pH over the temperature range of 5–40°C. Only at pH < 4 did these workers detect appreciable rod bending. Other studies based on viscoelastic[12] and electric birefringence[13] measurements yielded results indicating myosin rod to be only slightly flexible even at physiological temperatures.

There have been two differential scanning calorimetry (DSC) studies on the myosin rod flexibility problem. Potekhin et al.[14] investigated the thermal denaturation of rod and concluded that the rod had at least six quasi-independent cooperative domains. The region of lowest stability was placed near the middle of the rod. The work of Swenson and Ritchie[15] on S-2 showed a region of thermal instability corresponding to the hinge region.

In the present work we have determined the melting behavior of myosin rod and its two proteolytic fragments, long S-2 and LMM, by DSC in the pH range of 6.5–9.0 and in both phosphate and pyrophosphate buffers. The deconvoluted thermograms showed six two-state transitions for rod, either two or three two-state transitions for S-2, and five such transitions for LMM. These results enabled us to assign tentative locations of the two-state domains along the coiled-coil myosin rod.

MATERIALS AND METHODS

Proteins

Myosin was prepared from rabbit skeletal muscle as previously described.[16] Crude myosin rod, LMM, and S-2 were obtained by chymotryptic digestion of myosin or heavy meromyosin (HMM), as described by Margossian and Lowey.[17] In these procedures, rod was obtained by digestion of myosin filaments at 0.12*M* NaCl in the presence of EDTA, and LMM was obtained by digestion of soluble myosin at 0.5*M* KCl. Long S-2 was prepared from HMM that was obtained from chymotryptic digestion of soluble myosin at 0.5*M* KCl.

Two procedures were used to purify myosin rod. One was by Sephadex G-200 column chromatography (5 × 100 cm) in 50m*M* potassium phosphate at pH 7.0. The column-purified sample was dialyzed against 0.6*M* KCl, 50 m*M* potassium phosphate, pH 7.0, and 2 m*M* sodium azide (buffer A). Myosin rod purified in this way is referred to either as "native rod" or simply "rod." The other procedure involved denaturation of crude rod in 7*M* urea and purification of the denaturated protein, as described by Hvidt et al.,[12] in a 2.6 × 27 cm DEAE-cellulose (DE-52) column equilibrated in 7*M* urea, 25 m*M* Tris, pH 8.0, and 15 m*M* β-mercaptoethanol. The denatured protein was eluted with a linear gradient from 0 to 0.06*M* KCl, and renatured by dialysis against 0.6*M* KCl, 50 m*M* potassium phosphate, pH 7.3, 10 m*M* EDTA, and 1 m*M* DTT (dithiothreitol). The renatured rod was precipitated by dialysis against 30 m*M* KCl, 10 m*M* potassium phosphate, pH 7.0, and redissolved in buffer A. The rod sample prepared through a cycle of denaturation–renaturation in this way is referred to as "renatured rod." Both preparations were stored in 50% (V/V) glycerol at −20°C. LMM was purified in the same way as rod by G-200 chromatography. The purified protein was dialyzed against buffer A.

Long S-2 was chromatographed on a 2.6 × 60 cm Sephacryl S-200 column[17] equilibrated in 0.1*M* KCl, 20 m*M* potassium phosphate, pH 7.0, and 0.1*M* phenylmethane sulfonyl chloride (buffer B). The eluted S-2 was concentrated by precipitation at pH 4.5 and redissolved in buffer B plus 2 m*M* sodium azide.

Immediately prior to calorimetric studies, native rod was dialyzed against either 0.15*M* sodium pyrophosphate or 0.2*M* sodium phosphate and 0.5*M* KCl, pH 7.5, to remove glycerol, clarified by centrifugation at 20,000 × *g* for 15 min, and rechromatographed on a Sephadex G-200 column in the same buffer. The eluted rod was concentrated in polyethyleneglycol 2000 and clarified at 20,000 × *g* for 15 min. Other proteins were not rechromatographed, but were dialyzed against appropriate buffers used for calorimetric measurements. Polyacrylamide gels showed that rechromatographed native rod and the other proteins all migrated as one dominant band and were judged as electrophoretically homogeneous.

Protein concentrations were determined by measurements of absorbance at 280 nm. The following extinction coefficients and molecular weights[17] were used: 2.2 g^{-1} cm^{-1} for rod (MW 220,000), 3.0 g^{-1} cm^{-1} for LMM (MW 130,000), and 0.7 g^{-1} cm^{-1} for S-2 (MW 90,000). A value of 0.701 cm^3 g^{-1} was taken as the partial specific volume of these proteins.[17]

Calorimetric Measurements

Calorimetric experiments were carried out in a DASM-1M differential scanning calorimeter with 1-mL cells.[18] The heating rate was 1 K/min and the sample concentrations were in the range of 0.8–1.8 mg/mL. All proteins were studied in two buffers: (1) 0.5*M* KCl and 0.20*M* sodium phosphate, and (2) 0.5*M* KCl and 0.15*M* sodium pyrophosphate, both adjusted to the desired pH in the range of 6.5–9.0. The reversibility of thermal transitions was checked by reheating the samples immediately after cooling from the first scan. Reversibility was indicated when at least 50% of the melting curve was recovered in the second scan. Typically 65–75% recovery was obtained. However, higher protein concentrations, lower KCl concentrations, or pH values below 6.5 led to irreversible thermal unfolding. Rod and LMM were also judged irreversible at or above 1.5*M* KCl, but S-2 was still reversible at 1.5*M* KCl.

The total enthalpy of thermal transitions was determined from the areas under the excess heat capacity curves by using a 50 μW electrical calibration. The original tracings of apparent heat capacity were corrected for calorimetric (instrumental) baseline and for the difference in heat capacity between the initial and final states (chemical baseline). The resulting excess heat capacity functions were deconvoluted by using a multiple-pass deconvolution method,[19] which is based on the original algorithm proposed by Freire and Biltonen.[20,21] In this method the heat capacity curve is disentangled in a series of two-state transitions. As a final step the characteristic parameters defining each of the transitions were subjected to a nonlinear least-squares optimization.[19]

Reagents and Chemicals

α-Chymotrypsin was purchased from Worthington Diagnostic Systems (Freehold, NJ). DTT, phenylmethane sulfonyl chloride, and ultrapure ammonium sulfate were obtained from Sigma Chemical Co. (St. Louis, MO). Ultrapure urea was from Schwarz/Mann (Cleveland, OH). Sephadex G-200 and Sephacryl S-200 were obtained from Pharmacia (Piscataway, NJ), and DE-52 from Whatman BioSystems (Maidstone, England). All other chemicals used in this work were reagent grade or better.

RESULTS

Myosin Rod

Over the pH range studied (6.5–9.0) thermal denaturation of myosin rod, LMM, and S-2 was reversible. A typical DSC recording of the apparent heat capacity for rod is shown in Fig. 1 along with the trace obtained from reheating of the same sample. Four endothermic peaks are evident between 30 and 70°C. The general features of the melting profile are preserved on the remelting curve. The reversibility was observed with both native and renatured rod samples in the pH range of 6.5–9.0, but the denaturation became irreversible below pH 6.5. Figure 2 compares the melting curves for native and renatured rod at pH 7.5. The curves clearly indicate differences in the melting behavior of the two samples. The two peaks observed above 55°C in native

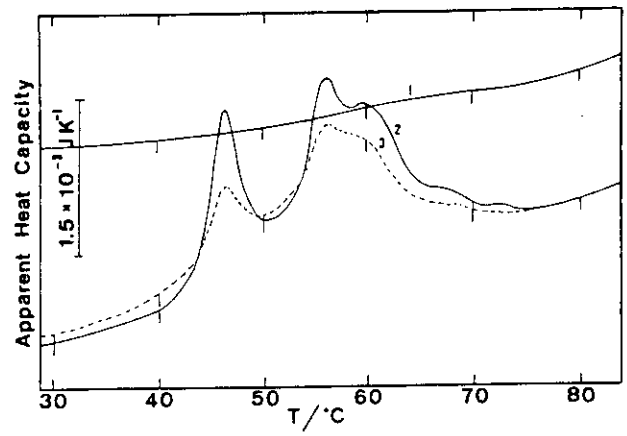

Fig. 1. Original DSC recording of myosin rod in 0.5*M* KCl, 0.15*M* sodium pyrophosphate, and pH 7.0. Rod concentration 1.7 mg/mL. Scan rate 1 K/min. Curve (1) baseline, (2) rod, and (3) remelting of the same sample used to obtain (2).

rod collapse into a single peak in renatured rod, whereas the other peak below this temperature is split into two peaks.

Figure 3 shows the apparent heat capacity curves for native rod determined in phosphate and pyrophosphate buffers. Both curves are qualitatively similar, although there are small differences in the apparent transition temperatures and the specific heat of denaturation (Δh). The differences were found for the entire pH range, as shown by the data given in Table I. The specific heats of denaturation for native rod determined in phosphate are in the range of 17–20 J/g for the six pH values studied, but the values in pyrophosphate are sensitive to alkaline pH and are considerably less than 17 J/g above pH 7.5. In contrast, higher Δh values are observed for renatured rod in pyrophosphate than in phosphate. The errors in these specific heats are estimated to be about 10%.

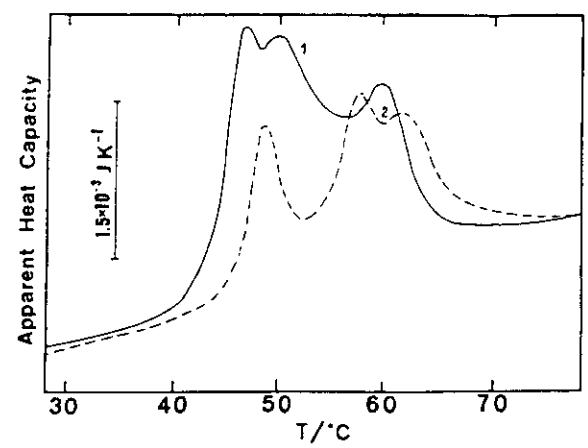

Fig. 2. Comparison of the DSC curves of renatured myosin rod (1) and native myosin rod (2). Both samples were in 0.5*M* KCl, 0.15*M* sodium pyrophosphate, and pH 7.5. Protein concentration: (1) 1.7 mg/mL and (2) 1.5 mg/mL. Scan rate was 1 K/min.

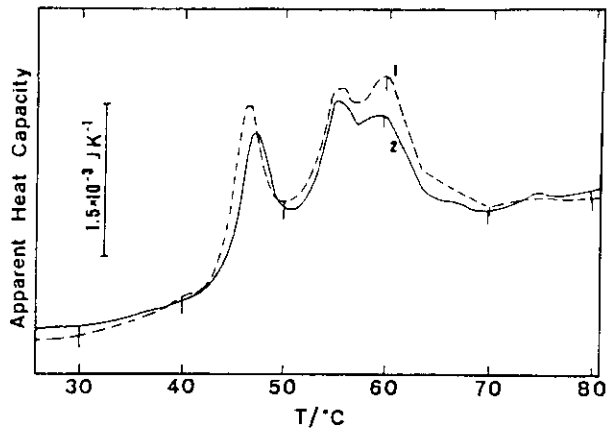

Fig. 3. Effect of buffers on the DSC curves of myosin rod in 0.5*M* KCl and pH 8.0; (1) 0.20*M* phosphate and (2) 0.15*M* pyrophosphate. Protein concentration was 1.8 mg/mL and scan rate was 1 K/min.

The heat capacity profiles of native rod determined in both buffers and different pH values were deconvoluted. The deconvoluted curve shown in Fig. 4 is for rod in phosphate at pH 7.0. Listed in Table II are the results of the deconvolution analysis of the DSC curves. Six endothermic peaks are resolved for the curves obtained in phosphate at all pH values. In pyrophosphate, six peaks are also resolved, but only in the pH range of 6.5–7.5. At higher pH, only five peaks are obtained. The peak that disappears at alkaline pH in pyrophosphate is either the 5th or 6th peak (above 60°C). The errors in the transition temperatures (T_i) are about 2°C and errors in the denaturation enthalpies (ΔH_i) could be as large as 100 kJ/mol. These relatively large errors could be due to (1) sample heterogeneity because rod was produced proteolytically and (2) low protein concentrations used in the measurements, which were necessary for avoiding aggregation but gave low signal : noise ratios. In addition, the complexity of the melting curves introduces a relatively large uncertainty in the correction for the difference in heat capacity between the initial and final states (a necessary and critical step in the deconvolution procedures[19]). Individual transition temperatures vary by only two degrees across the pH range in phosphate. The variations in each transition enthalpy

TABLE I
Specific Heat of Denaturation of Myosin Rod[a]

pH	Δh (Phosphate)		Δh (Pyrophosphate)	
	Native	Renatured	Native	Renatured
6.5	19.0		17.4	
7.0	19.8	21.0	17.8	24.4
7.5	17.4	18.0	17.6	24.0
8.0	18.4	18.8	12.6	21.5
8.5	17.4		14.2	
9.0	18.1		10.6	

[a]Specific heats of denaturation (Δh) are in J/g. Rod was in 0.5*M* KCl and either 0.20*M* sodium phosphate or 0.15*M* sodium pyrophosphate.

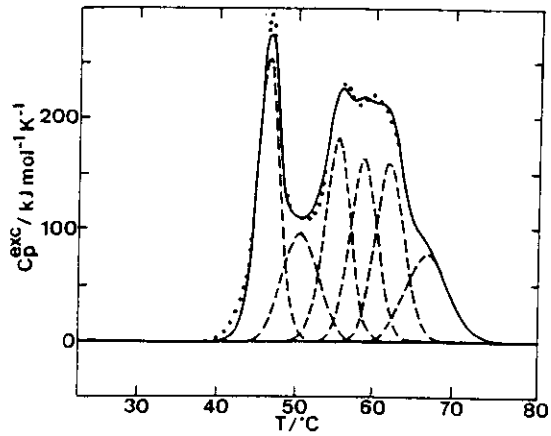

Fig. 4. Computer deconvolution of the excess heat capacity function of myosin rod in 0.5*M* KCl, 0.2*M* phosphate, and pH 7.0. (·····) Experimental curve, (----) resolved individual components, and (———) sum of the six resolved transitions.

are as large as 180 kJ/mol from pH 7.0 to 9.0, with the difference being 100–150 kJ/mol for five of the peaks. There are no apparent systematic variations of the enthalpies with pH. These results suggest that the melting characteristics of rod in phosphate are not very sensitive to pH, in agreement with the small variations of specific heats of denaturation as a function of pH in this buffer (Table I). In pyrophosphate, the variations in transition temperatures between pH 6.5 and 9.0 are slightly larger (4°C). The variations in individual transition enthalpies across the pH range are also larger, in the range of 200–300 kJ/mol for transitions 2–6. For the first transition, the difference in ΔH_1 between pH 6.5 and 9.0 is 575 kJ/mol.

The van't Hoff enthalpy (ΔH_{VH}) for each of the resolved transitions shown in Fig. 4 was calculated from the pH 7 phosphate data listed in Table II and the maximum value of the heat capacity function. The ratio of the calculated

TABLE II
Deconvolution of Specific Heat Function of Myosin Rod[a]

Buffer	pH	T_1	ΔH_1	T_2	ΔH_2	T_3	ΔH_3	T_4	ΔH_4	T_5	ΔH_5	T_6	ΔH_6
Phosphate	7.0	46	917	51	596	55	800	59	755	62	734	67	546
	7.5	46	810	51	510	55	751	59	641	62	633	68	482
	8.0	45	768	51	607	54	697	58	701	61	555	67	398
	8.5	47	806	50	501	55	724	58	624	61	721	66	457
	9.0	47	824	50	542	55	752	59	702	62	709	68	462
Pyrophosphate	6.5	46	895	52	591	55	685	58	596	63	627	67	426
	7.0	47	840	52	536	56	811	60	686	63	596	69	455
	7.5	47	664	48	519	54	603	57	770	60	794	65	510
	8.0	47	699	52	397	56	656	60	628	—	—	65	384
	8.5	47	696	49	694	54	732	59	531	61	479	—	—
	9.0	44	320	48	600	55	556	60	578	—	—	68	288

[a] Transition temperatures (T_i) are in degrees centigrade. Heats of denaturation (ΔH_i) are in kJ/mol. Native myosin rod was in 0.5*M* KCl and either 0.20*M* sodium phosphate or 0.15*M* sodium pyrophosphate.

TABLE III
Specific Heat of Denaturation of LMM[a]

pH	Δh (Phosphate)	Δh (Pyrophosphate
6.5	18.4	21.0
7.0	23.9	22.2
7.5	19.9	25.2
8.0	16.0	22.3
8.5	16.7	22.0
9.0	20.8	21.8

[a]Specific heats of denaturation (Δh) are in J/g. LMM was in 0.5M KCl and either 0.20M sodium phosphate or 0.15M sodium pyrophosphate.

van't Hoff enthalpy to calorimetric enthalpy ($\Delta H_{VH} : \Delta H_d$) was found to be 1.0, 0.9, 1.0, 1.0, 1.1, and 1.0 for the six transitions. These values are expected since the deconvolution method is based on the assumption of two-state transitions. The ratios for the other transitions shown in Table II are all very close to unity, in the range of 0.9–1.1. Thus melting of rod involves several states and each of the transitions can be approximated by a two-state process.

Rod Fragments

As with native rod, the specific heat of denaturation for LMM in phosphate is relatively insensitive to pH (Table III). The mean value for six pH values is 19.3 J/g as compared to the mean of 18.4 J/g for native rod. In pyrophosphate the specific heat is also relatively constant and is not reduced at high pH. For the pH range of 6.5–7.5, the mean value (22.4 J/g) of LMM in pyrophosphate is substantially higher than the mean (17.6 J/g) for rod.

The deconvoluted DSC curves for LMM in pyrophosphate at pH 8.0 is shown in Fig. 5. The curve is resolved into four endothermic transitions in the range of 40–70°C. Table IV summarizes the deconvolution results of LMM. Of

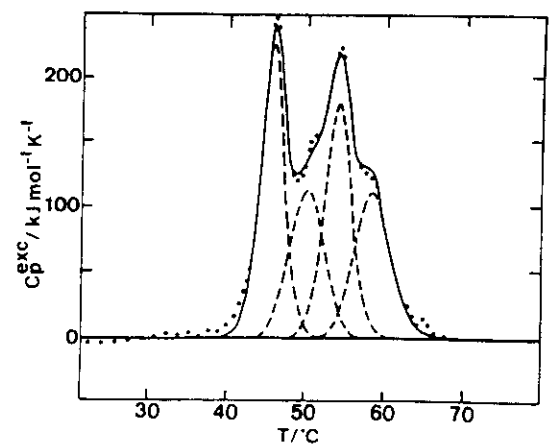

Fig. 5. Computer deconvolution of the excess heat capacity function of LMM in 0.5M KCl, 0.15M sodium pyrophosphate, and pH 8.0. (· · · · ·) Experimental curve, (- - - - -) resolved individual components, and (——) sum of the four resolved transitions.

TABLE IV
Deconvolution of Specific Heat Function of LMM[a]

Buffer	pH	T_0	ΔH_0	T_1	ΔH_1	T_2	ΔH_2	T_3	ΔH_3	T_4	ΔH_4	T_5	ΔH_5
Phosphate	6.5			44	785	53	482	56	642	61	484	—	—
	7.0			45	828	51	536	55	768	60	560	66	411
	7.5			45	778	52	430	54	745	60	489	—	—
	8.0			46	645	—	—	54	689	59	444	65	308
	8.5			46	702	53	511	54	490	61	470	—	—
	9.0			46	772	52	565	55	748	60	616	—	—
Pyrophosphate	6.5			45	810	53	573	56	762	62	586	—	—
	7.0			46	859	53	603	56	784	61	640	—	—
	7.5			46	887	51	646	54	810	59	625	64	306
	8.0			46	870	50	619	54	776	59	638	—	—
	8.5	46	390	47	700	52	586	56	723	61	566	—	—
	9.0			47	797	50	617	54	813	59	601	—	—

[a]Transition temperatures (T_i) are in degrees centigrade. Heats of denaturation (ΔH_i) are in J/mol. LMM was in 0.5*M* KCl and either 0.20*M* sodium phosphate or 0.15*M* sodium pyrophosphate.

the twelve DSC curves, nine are resolved into four peaks, while three curves show a fifth peak. For the four main transitions (1–4), the variations in transition temperatures across the pH range are 3°C or less, and the variations in enthalpies are either comparable to or less than the variations observed for rod. There is no anomaly in any of the observed enthalpies at pH 9.0 in pyrophosphate. These results suggest that melting of LMM is not pH sensitive in either phosphate or pyrophosphate. The ratios ΔH_{VH} : ΔH_d were 1.0, 1.0, 1.1, and 1.0 for the four LMM transitions shown in Fig. 5, indicating the two-state nature of each of the transitions. Similar ratios were obtained for the entire pH range in both buffers.

The specific heats of denaturation for S-2 are given in Table V. These values are smaller than those observed for LMM or rod. Figure 6 shows the deconvoluted heat capacity function for S-2 in phosphate at pH 7.0. The deconvolution parameters for this and other pH values are listed in Table VI. Most of the DSC curves are resolved into two main transitions. For four of the twelve sets of experimental conditions, a third small peak appears at both high and low pH values. Across the pH range of 6.5–9.0 the enthalpies of the

TABLE V
Specific Heat of Denaturation of S-2[a]

pH	Δh (Phosphate)	Δh (Pyrophosphate)
6.5	13.8	14.7
7.0	8.6	9.9
7.5	7.2	8.2
8.0	5.8	7.4
8.5	13.3	12.8
9.0	11.2	11.9

[a]Specific heats of denaturation (Δh) are in J/g. S-2 was in 0.5*M* KCl and either 0.20*M* sodium phosphate or 0.15*M* sodium pyrophosphate.

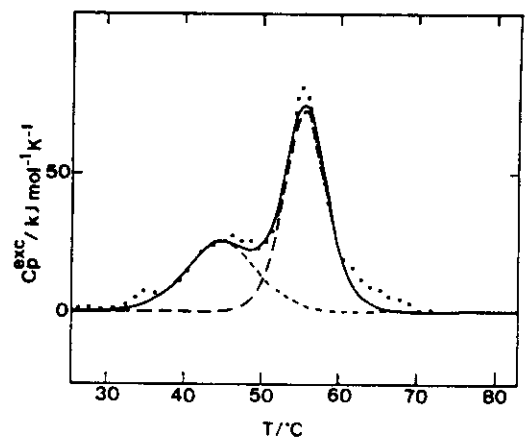

Fig. 6. Computer deconvolution of the excess heat capacity function of S-2 in 0.5*M* KCl, 0.2*M* sodium phosphate, and pH 7.0. (· · · · ·) Experimental curve, (- - - -) resolved individual components, and (———) sum of the two resolved curves.

TABLE VI
Deconvolution of Specific Heat Function of S-2[a]

Buffer	pH	T_0	ΔH_0	T_1	ΔH_1	T_2	ΔH_2	T_3	ΔH_3
Phosphate	6.5			47	345	56	568	59	329
	7.0			46	284	57	493	—	—
	7.5			45	227	57	119	—	—
	8.0			48	172	57	350	—	—
	8.5			47	344	57	557	60	291
	9.0			47	322	58	689	—	—
Pyrophosphate	6.5	41	370	51	469	54	470	—	—
	7.0			49	270	57	510	—	—
	7.5			47	288	56	446	—	—
	8.0			46	272	56	393	—	—
	8.5	41	288	47	342	56	522	—	—
	9.0			47	318	58	548	63	209

[a] Transition temperatures (T_i) are in degrees centigrade. Heats of denaturation (ΔH_i) are in kJ/mol. S-2 was in 0.5*M* KCl and either 0.20*M* sodium phosphate or 0.15*M* sodium pyrophosphate.

two main transitions (ΔH_1 and ΔH_2) are smaller at pH 7.5 and 8.0 than lower or higher pHs, with a minimum value at pH 8.0. These results reflect the effect of pH on specific heats (Table V). Within the pH range of 7.0–8.0 the specific heats are below 10 J/g in both buffers, whereas they are 11–15 J/g at lower and higher pH values. This pH effect was not detected in intact rod or LMM.

DISCUSSION

We have examined the thermal unfolding of myosin rod and two of its proteolytic fragments by DSC over a wide pH range and in moderate ionic strength. The results reported here were obtained under conditions in which a reasonable thermal reversibility was obtained. The irreversibility observed below pH 6.5 likely arises from acid aggregation as the pH approaches the

TABLE VII
Mean Transition Temperatures and Heats of Denaturation[a]

Transition	Transition Temperature (°C)	ΔH (kJ/mol)
	Phosphate	
1	46.2 ± 0.8	825 ± 55
2	50.6 ± 0.5	551 ± 48
3	54.8 ± 0.5	745 ± 38
4	58.6 ± 0.6	685 ± 53
5	61.6 ± 0.5	670 ± 76
6	67.2 ± 0.8	469 ± 61
	Pyrophosphate	
1	46.3 ± 1.2	686 ± 201
2	50.2 ± 2.0	556 ± 99
3	55.0 ± 0.9	674 ± 91
4	59.0 ± 1.3	632 ± 85
5	61.7 ± 1.5	635 ± 132
6	68.8 ± 1.8	413 ± 83

[a] The transition temperatures and ΔH values observed for each melting peak shown in Table II were averaged over the pH range studied. The uncertainty for each mean value is the standard deviation.

isoelectric point. The apparent heat capacity vs temperature curves for myosin rod show complex features. These curves have been deconvoluted into six two-state transitions by a multipass procedure in which the transition parameters are optimized. The deconvolution provides confidence that the unfolding of rod proceeds by melting several independent cooperative domains.

The unfolding of myosin rod in phosphate is relatively insensitive to pH within the range of 7.0–9.0 with respect to transition temperature, transition enthalpy, and the number of independent cooperative two-state transitions. The mean transition temperature and enthalpy for each transition are summarized in Table VII. The variation of individual ΔH_i values for each transition over the pH range is 16–37%, and the standard deviations of the variations are in the range 5–13% of the mean values. The mean and standard deviation of the total enthalpy for five pH values is 3945 ± 244 kJ/mol. At 20°C the heat capacity values are ca 1.7 J/g-K. This value is substantially higher than the average value (ca 1.3 J/g-K) for globular proteins.[18] The difference might be interpreted as reflecting the large number of vibrational modes and of contacts between hydrophobic residues and solvent, following the arguments of Sturtevant.[22]

The melting profiles of rod in pyrophosphate are more variable across the pH range of 6.5–9.0. One of the two high-temperature transitions disappears at alkaline pH. The reason for this is unclear. The enthalpy for transition 1 in pyrophosphate is considerably smaller at pH 9.0 than at lower pH values. The standard deviation of enthalpy for this transition (ΔH_1) is 30% of the values averaged over the pH range (Table VII), considerably larger than for the other transitions (13–21% of the mean values). There appears to be a significant pH effect on the unfolding enthalpy of rod in the presence of 0.15M sodium pyrophosphate. T_1 at pH 9.0 is 2–3 degrees lower than at higher pH values. The threefold decrease in the enthalpy of transition 1 at pH 9.0 may

reflect an inherent disordered structure in domain 1 that is not present in the other domains. This disordered structure might be enhanced by the specific solvent conditions.

We now consider the results obtained at pH 7.0 in phosphate buffer. The results for rod are generally comparable to those previously obtained under similar (0.5*M* KCl, 0.02*M* phosphate, pH 6.5, and 2–4 mg/mL protein) but not identical conditions by Potekhin et al.[14] Their deconvoluted results[23] showed six transitions with transition temperatures at 43, 48, 50, 51, 56, and 61°C, and corresponding enthalpies of 820, 440, 710, 760, 680, and 490 kJ/mol. The sum of these enthalpies is 3900 kJ/mol as compared with the total enthalpy of 4400 kJ/mol observed in the present work. The latter value is in reasonable agreement with the sum of the enthalpies for LMM and S-2 (3900 kJ/mol). The present transition temperatures are several degrees higher t' the previous results, but the enthalpies may be considered in reasonable agreement considering their relatively large errors. The previous study[14] was carried out at higher protein concentrations and lower ionic strength. These conditions could lead to irreversible thermal unfolding and account for the observed differences in melting temperatures. It should be noted that the present study is the first in which the DSC transitions for myosin rod and its fragments are reported to be reversible. This reversible character is a necessary condition to properly apply any method for deconvolution analysis and implies the existence of thermodynamic equilibrium throughout the overall denaturation process.[21]

The transition temperatures observed at pH 7.0 and phosphate for all three proteins are aligned in Table VIII. The fourth transition of rod is evident in S-2, but not in LMM. The second S-2 transition may be assigned to domain 4 in rod. This assignment is supported by previous results (see below). The assignment of the first transition of S-2 is less straightforward. The two heavy chains of myosin are organized into a two-stranded coiled-coil α-helix at the C-terminal half. The coiled-coil structure extends from the C-terminus to about 150 nm, at which each of the two polypeptide chains folds into a globular domain (the myosin head or S-1 moiety) in which two light ch s are bound. The hinge region in the coiled-coil structure (rod) is flanked by the LMM segment at the C-terminal end and the S-2 segment at the N-terminal end. Long S-2, which can be obtained by proteolytic digestion of HMM and was used in the present work, contains the coiled-coil S-2 segment (short S-2) and a part of or the entire hinge region located adjacent to the C-terminal end of short S-2. The enthalpy for the 46°C transition of long S-2 accounts for 32%

TABLE VIII
Comparison of DSC Transition Temperatures of Myosin Rod, LMM, and S-2[a]

	Transition Domains					
	1	2	3	4	5	6
Rod	46	51	55	59	62	67
LMM	45	51	55	—	60	66
Long S-2	46	—	—	57	—	—

[a]Transition temperatures are in degrees centigrade. These data are for the proteins in 0.5*M* KCl, 0.20*M* sodium phosphate, and pH 7.0.

of the total enthalpy for the S-2. On the basis of the masses of long and short S-2, the hinge region constitutes about one-third of long S-2. The hinge region is known to have a lower thermal stability than the flanking LMM or short S-2.[15] In the latter work two transitions were observed for long S-2 and only one transition was detected for short S-2, in which the low-temperature transition observed with long S-2 disappeared. By a combination of optical rotation and temperature-jump measurements, Tsong[26] showed that the hinge region had a lower thermal stability than short S-2 and the melting of the hinge region was dominated by a fast relaxation process. Thus the 46°C transition of our long S-2 may be assigned unambiguously to the unfolding of the hinge region and the 57°C transition to the melting of the short S-2 segment. Our DSC transition temperatures for long S-2 are higher than those previously reported,[15] but it should be noted that the previous study was carried out under somewhat different conditions (0.2*M* KCl, 0.02*M* phosphate, pH 7.0) and the DSC curves were not deconvoluted. The present enthalpy of the high-temperature transition is 5 J/g and that of the other transition is 3 J/g at pH 7.0. These results are in the same range reported by Swenson and Ritchie.[15]

The lowest transition temperatures observed for rod, LMM, and long S-2 are in the range of 45–46°C. The structural domain giving rise to this transition in each fragment must be the least stable domain of that protein. The assignment of the least stable transition of long S-2 to the hinge region is relatively uncomplicated, but the relationship between this transition and the transitions observed with rod and LMM is not immediately obvious. Because of the coincidence in their transition temperatures, transition 1 in rod may be considered as a composite transition reflecting transition 1 of LMM and transition 1 of long S-2. In this model, ΔH_1 for rod would be larger than ΔH_1 for LMM or ΔH_1 for long S-2, and would be the sum of the latter two enthalpies. The molar ΔH_1 for rod is smaller than ΔH_1 (LMM) + ΔH_1 (S-2) by some 20%. We cannot be certain that our S-2 actually contained the entire hinge region. If it contained only a part of the entire hinge region, then the molar ΔH_1 for the S-2 would be smaller than 284 kJ/mol. This smaller value would reduce the difference between ΔH_1 (rod) and the sum of the other two values. Such a structure would require domain 1 of rod to contain both the hinge region susceptible to proteolysis and a region resistant to proteolysis. Both regions would have about equal thermal stability. There is additional evidence in favor of the assignment of domain 1 to the hinge region or the S-2/LMM junction. The enthalpy of transition 1 is threefold decreased from pH 6.5–9.0 in pyrophosphate, but such a pronounced pH/pyrophosphate effect is not observed for any of the transitions of LMM or long S-2. The absence of this effect in the other two fragments could be explained if domain 1 contains the S-2/LMM junction. Its thermal properties are altered upon proteolytic cleavage at a point within the domain.

Potekhin et al.[14] observed two transitions for a segment of LMM (LF_3) that was obtained by digestion of LMM and was the C-terminal half of LMM. They assigned these two transitions (51 and 56°C) to domains 3 and 5 in rod on the basis of similar transition temperatures. If the present domains 3 and 5 are identified with those reported by Potekhin et al. as located at the C-terminal end, domains 2 and 6 may be located near the middle of the rod structure, as depicted in Fig. 7. If domain 2 is placed adjacent to domain 1,

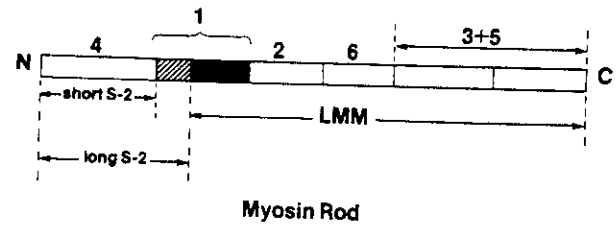

Fig. 7. Cooperative domains in myosin rod suggested by DSC data obtained at pH 7.0, 0.5*M* KCl, and 0.2*M* sodium phosphate. The N-terminal end is the head–rod junction. The numbers 1–6 denote domains of increasing thermal stability. Cleavage within the most unstable domain 1 results in long S-2 and LMM. Domains 2 and 6 are located in the middle, and their positions be reversed. Domains 3 and 5 are located at the C-terminal segment, but it is not certain which domain is at the end (after Ref. 14 for the locations of domains 3 and 5).

then the two most unstable domains are contiguous occupying a segment beginning at a point about 20% of the length of rod from the head–rod junction (N-terminal end of rod) to a point near the middle of the rod. If domain 6 is placed adjacent to domain 1, then the second most unstable region lies just beyond the middle of the rod and is separated from the most unstable domain by the most stable domain. Rodgers and Harrington[10] recently showed that the radius of gyration of rod (ca 35 nm) observed under hinging conditions (0.6*M* NaCl and 0.02*M* phosphate, or 0.5*M* KCl and 0.5*M* phosphate, neutral pH, and 20–40°C) can be explained by either a central hinge or a hinge located at a point one-third from the head–rod junction. The locations of domains 1 and 2 shown in Fig. 7 are compatible with these findings. Our model differs from an early one in two aspects. The previous investigators[14] placed domains 1 and 2 together near the middle of the rod away from the hinge region. The present results cannot be easily reconciled with the most unstable domain 1 placed near the middle of the rod because long S-2 does not extend beyond about 50 nm from the N-terminus. Our model suggests that domain 1 encompasses a segment that extends into the C-terminal end of LMM. If the entire domain 1 corresponds to the thermally unstable hinge region, the size of this region is larger than previously thought. If the six two-state transitions reflect six independent domains, the experimental mean residue specific heats of denaturation are expected to be additive. As an approximation, the specific heats (Δh) given in Table I for rod should be equal to (130,000/220,000)Δh for LMM + (90,000/220,000)Δh for S-2. This equality holds to within 15% (4–15%) for the specific heats obtained in both phosphate and pyrophosphate in the pH range of 6.5–7.5. Under these experimental conditions the melting of the domains is likely independent of one another.

LMM unfolds in phosphate and pH 7.0 in a manner very similar to rod. Transition 4, which has been attributed to the melting of the helical short S-2 segment, is not detected in LMM. The transition temperatures and the enthalpies are reasonably similar for rod and isolated LMM. The structure of the isolated fragment appears approximately the same as when it is part of the intact rod. The properties of isolated long S-2 are considerably different from those of S-2 observed in intact rod. In both phosphate and pyrophosphate the two observed enthalpies are lower than those for domains 1 and 4 in rod.

Figure 7 is proposed on the basis of data obtained in phosphate at pH 7.0. These are the conditions most similar to those used by previous investigators for DSC and other melting studies. The presence of two thermally unstable regions located away from the ends provides a mechanism by which myosin rod can hinge. The results obtained at other pH values or in pyrophosphate are not always consistent with Fig. 7. Under certain conditions only four instead of five endotherms are detected with LMM. An occasional third (high-temperature) peak appears in the thermal profile of S-2 in phosphate at low and high pH. In pyrophosphate both a third low-temperature or a third high-temperature peak is observed, again at low or high pH. Because of the apparent complexity of these data, we have not integrated them into the general discussion and have not attempted an interpretation.

After the present work was completed, two abstracts on DSC studies of myosin fragments appeared. Shriver et al.[27] reported two endothermic peaks (41 and 48°C) for the melting of HMM in 0.1*M* KCl, 25 m*M* Tris, pH 7.9, and assigned the low-temperature peak to the unfolding of the S-2 domain (short S-2) on the basis of the DSC curves of long S-2. This study also indicated that the melting curves of LMM contained at least four endothermic peaks. Bertazzon et al.[28] observed six two-state thermal transitions with myosin rod in 0.1*M* KCl and phosphate at pH 7.0. Their transition temperatures were in the range of 42–55°C and the enthalpies for the six peaks (with increasing transition temperatures) were 840, 660, 995, 602, 681, and 518 kJ/mol. Consistent with our data obtained in phosphate and pH 7.0, their first endotherm (42°C) accounted for 20% of the total enthalpy and the sixth peak was the smallest, accounting for 12%. In spite of the differences in ionic strength and chloride concentration, the agreement on the enthalpies of myosin rod between our results and those of Bertazzon et al. is good.

We have consistently observed higher transition temperatures for all three myosin fragments than reported by other investigators.[14,15,27,28] It was shown by Stafford[29] that increasing chloride concentration in the range of 0–0.6*M* stabilized the major portion of the rod coiled-coil, but destabilized the S-2/LMM junction. These studies were carried out by CD and proteolytic digestion of rod. Since our solution contained 0.5*M* KCl and the other DSC studies were done in 0.1*M* KCl, this difference could account for the higher transition temperatures reported here. The transition temperature for transition 1 of rod under our solvent conditions is only 2–4°C higher than the corresponding transition observed in the other two studies of myosin rod, but the transition temperatures for the other peaks are substantially higher. This is also true for LMM and S-2. If our chloride concentration is indeed responsible for the observed higher thermal stability of domains 2–5, then the small difference in the transition temperature for transition 1 may actually reflect destabilization of domain 1 by 0.5*M* chloride. This interpretation is compatible with the assignment of domain 1 to the hinge region and the S-2/LMM junction.

The deconvoluted DSC curves of myosin rod are considerably more complex than melting curves obtained from optical rotation or CD measurements. In general, only two transitions are evident from these data in moderately high chloride concentrations (up to 0.6*M*). Derivative plots[10] of the optical rotation profiles showed two peaks at 47 and 55°C in 0.6*M* NaCl, 0.02*M* phosphate, and pH 7.0, and curve fittings[29] of the melting profiles obtained in 0.6*M* NaCl,

0.005*M* phosphate, and pH 7.3 also yielded two transitions at 45 and 53°C. It is of interest to relate these spectroscopic transitions to calorimetric transitions. Transition 5 reported here and by others[23,28] has an enthalpy of 680–740 kJ/mol, and accounts for 16–17% of the total enthalpy. These values correlate well with the high-temperature transition obtained from derivative plots, as has been pointed out previously.[10] Thus the high-temperature spectroscopic transition of myosin rod may involve unfolding of a single domain near the C-terminal end. Rodgers and Harrington[10] have suggested that their low-temperature transition may involve the melting of several domains, including the hinge region. The melting of these domains cannot be resolved by optical rotation. When the phosphate concentration was increased to 0.5*M*, the fractions of the two transitions were reversed with the high-temperature transition containing 69% (instead of 20%) of the structure. The stabilization by high ionic strength involves several domains, and the transitions of these domains cannot be resolved. On the other hand, Stafford[29] has attributed the low-temperature peak observed by him to calorimetric transition 1 reported by Privalov[23] on the basis of equal enthalpies, and indicated no correspondence between his high-temperature transition (enthalpy 250 kJ/mol) and any of the other five calorimetric transitions. Again, multiple transitions cannot be resolved by an optical method. Because the effects of ionic strength and chloride concentration on the thermal stability of the various domains of myosin rod are complex, it is difficult to disentangle these effects and to correlate calorimetric transitions with spectroscopic transitions without further studies under equivalent solvent conditions.

The difference in the apparent heat capacity profile between native and renatured rod is visibly pronounced. Previous studies detected no significant difference between these two types of myosin rod in terms of ultracentrifugation results, intrinsic viscosity, and uv spectrum.[12] The present results suggest that rod purified by Sephadex G-200 may have a different conformation from rod purified by a cycle of denaturation–renaturation followed by Sephacryl S-200 column chromatography. The present data are limited to one solvent condition in which the calorimetric measurements were obtained. We have no information at this time as to whether the apparent differences may persist under other conditions.

In summary, we have investigated the thermal unfolding of myosin rod, LMM, and long S-2 in two buffers systems and over a wide pH range. Based on data obtained at pH 7.0 in phosphate, myosin rod has been shown to contain six independent cooperative domains, each of which can undergo a two-state thermal transition. We suggest that the most unstable domain includes the hinge region located adjacent to the C-terminal end of the α-helical short S-2 segment and a small N-terminal segment of LMM. This domain contains the S-2/LMM junction at which LMM can be cleaved from S-2 or from HMM. The proposed locations of the two most unstable domains within myosin rod can give rise to a flexible coiled-coil structure compatible with a hinging myosin rod. Calorimetric data alone, however, provide no indication of the relative stiffness of the hinge. In a recent study, Lovell et al.[30] showed that the isometric force of skinned muscle fibers was greatly suppressed by polyclonal antibody directed against S-2. While the physiological significance of this effect is not yet fully understood, the results point to a

role of the S-2 segment in the contractile cycle. If rod hinging in filamentous structure can be induced by a reversible two-state transition that occurs within the S-2 region and if this transition plays an active role in contraction, it would seem important to consider the energetic relationship between hinging and tension development. Other studies will be required to address this problem.

This work was supported in part by grants INT 8420897 (H. C. C. and M. C.) from the National Science Foundation (U.S.-Spain Joint Committee for Scientific and Technological Cooperation) and AR31239 (H. C. C.) from the National Institutes of Health, and 1233/84 from CAICTT (Spain). J. L. L. L. acknowledges a PFPI fellowship. The authors thank one of the referees for specific suggestions that led to improvement of the manuscript.

References

1. Huxley, H. E. (1960) *Science* **164**, 1356–1366.
2. Huxley, H. E. & Simmons, R. M. (1971) *Nature* **233**, 533–538.
3. Harrington, W. F. (1971) *Proc. Natl. Acad. Sci. USA* **68**, 685–689.
4. Harrington, W. F. (1979) *Proc. Natl. Acad. Sci. USA* **76**, 5066–5070.
5. Harvey, S. C. & Cheung, H. C. (1982) in *Cell and Muscle Motility*, Dowben, R. M. & Shay, F. W., Eds., Plenum Press, New York, pp. 279–302.
6. Harrington, W. F. & Rodgers, M. E. (1984) *Ann. Rev. Biochem.* **53**, 35–74.
7. Burke, M., Himmelfarb, S. & Harrington, W. F. (1973) *Biochemistry* **12**, 701–710.
8. Highsmith, S., Kretzchmar, K. M., O'Konski, C. T. & Morales, M. F. (1977) *Proc. Natl. Acad. Sci. USA* **74**, 4986–4990.
9. Highsmith, S., Wang, C. C., Zero, K., Pecora, R. & Jardetzky, O. (1982) *Biochemistry* **21**, 1192–1197.
10. Rodgers, M. E. & Harrington, W. F. (1987) *Biochemistry* **26**, 8697–8730.
11. Harvey, S. C. and Cheung, H. C. (1977) *Biochemistry* **16**, 5181–5187.
12. Hvidt, S., Nestier, F. H. M., Greaser, M. L. & Ferry, J. D. (1982) *Biochemistry* **21**, 4064–4073.
13. Hvidt, S., Chang, T. & Yu, H. (1984) *Biopolymers* **23**, 1283–1294.
14. Potekhin, S. A., Trapkov, V. A. & Privalov, P. L. (1979) *Biofizika* **24**, 46–50.
15. Swenson, C. A. & Ritchie, P. A. (1980) *Biochemistry* **19**, 5371–5375.
16. Aguirre, R., Gonsoulin, F. & Cheung, H. C. (1986) *Biochemistry* **25**, 6827–6835.
17. Margossian, S. S. & Lowey, S. (1982) *Methods of Enzymol.* **85**, 55–71.
18. Privalov, P. L. & Khechinashvili, N. N. (1974) *J. Mol. Biol.* **86**, 665–684.
19. Baron, C., Freire, E., Mateo, P. L. & Cortijo, M. (1985) *Acta Cient. Compost.* **22**, 303–317.
20. Biltonen, R. L. & Freire, E. (1978) *Crit. Rev. Biochem.* **5**, 85–124.
21. Freire, E. & Biltonen, R. L. (1978) *Biopolymers* **17**, 463–479.
22. Sturtevant, J. M. (1977) *Proc. Natl. Acad. Sci. USA* **74**, 2236–2240.
23. Privalov, P. L. (1982) *Adv. Protein Chem.* **35**, 1–104.
24. Sutoh, K., Sutoh, K., Karr, T. & Harrington, W. F. (1978) *J. Mol. Biol.* **126**, 1–22.
25. Ueno, H. & Harrington, W. F. (1984) *J. Mol. Biol.* **180**, 667–701.
26. Tsong, T. Y. (1983) *J. Mol. Biol.* **164**, 431–450.
27. Shriver, J. W., Zegar, I. & Kamath, U. (1988) *Biophys. J.* **53** (no. 2, part 2), 236a.
28. Bertazzon, A., Tian, G. H. & Tsong, T. Y. (1988) *Biophys. J.* **53** (no. 2, part 2), 236a.
29. Stafford, W. F., III (1985) *Biochemistry* **24**, 3314–3321.
30. Lovell, S., Karr, T. & Harrington, W. T. (1988) *Proc. Natl. Acad. Sci. USA* **85**, 1849–1853.

Received October 6, 1988
Accepted December 15, 1988

ELSEVIER

FEBS Letters 344 (1994) 154–156

FEBS 13973

FEBS LETTERS

The thermodynamics of the unfolding of an isolated protein subdomain

The 255–316 C-terminal fragment of thermolysin

Francisco Conejero-Lara[a], Vincenzo De Filippis[b], Angelo Fontana[b], Pedro L. Mateo[a,*]

[a]*Department of Physical Chemistry, Faculty of Sciences, and Institute of Biotechnology, University of Granada, 18071 Granada, Spain*
[b]*CRIBI Biotechnology Centre, University of Padua, 35121 Padua, Italy*

Received 23 March 1994

Abstract

Differential scanning calorimetry has been used to study the thermal unfolding of the 255–316 C-terminal fragment of thermolysin. The concentration effect on the calorimetric transitions of the fragment in 0.1 M NaCl and 20 mM phosphate buffer, pH 7.5, shows that it behaves as a highly stable dimer in solution, whithin the concentration range 0.19–4.55 mg/ml, undergoing a reversible two-state thermal unfolding process. The thermodynamic parameters of unfolding (ΔG = 60 ± 6 kJ/(mol of dimer) at 20°C) are similar to those normally observed for small, compact, globular proteins. This and previous studies [1989, Eur. J. Biochem. 180, 513–518] show that the 255–316 fragment folds into a stable, native-like globular structure.

Key words: Differential scanning colorimetry; Thermolysin; Protein stability; Protein domain; Domain folding

1. Introduction

That relatively large proteins have a discrete structure is nowadays well accepted, since proteins of more than 100 amino acid residues are usually composed of domains and subdomains. This can be seen by X-ray [1,2] or computational [3–6] analysis, as well as by studying the folding properties of protein fragments corresponding to domains in the intact protein ([7] and references cited therein). The 316-residue chain of thermolysin [EC 3.4.24.4] was shown by X-ray analysis to be composed of two similar structural domains (1–157 and 158–316) [8] and computational approaches described the hierarchic architecture of the protein ranging from secondary-structure, element-folding units to whole protein subdomains [9–11]. The location of domains and subdomains in thermolysin has been studied experimentally by examining the folding and stability properties of its chemical and proteolytic fragments [12–15]. Circular dichroism and immunochemical measurements showed that some C-terminal fragments adopt stable globular conformations in water, similar to the corresponding regions in the native protein [16]. The 255–316 thermolysin fragment was shown to fold independently into a stable, native-like conformation [17]. This fragment dimerizes when dissolved in aqueous buffer at concentrations higher than 0.1 mg/ml [18]. Circular dichroism studies show, however, that dimerization does not lead to alterations of fragment secondary structure, thus signifying that the association process is not critical for dictating the native-like folding of the fragment [18].

High-sensitivity differential scanning calorimetry (DSC) is a very appropriate technique for characterizing the energetics of the thermal unfolding of proteins, and may lead to the analysis of association processes, as long as the overall denaturation process occurs under equilibrium conditions [19,20]. DSC has been used here to study the thermal stability of the 255–316 thermolysin fragment at pH 7.5. The thermal unfolding of the 255–316 fragment has proved to be a highly reversible process. An analysis of the concentration effect on the DSC traces is consistent with a dimeric fragment undergoing two-state unfolding with no intermediate states according to the scheme $F_2 \rightleftharpoons 2U$. The thermodynamic parameters of the unfolding process are characteristic of a compact globular structure for the dimer.

2. Materials and methods

Thermolysin was bought from Sigma as a crystallized and lyophilized powder. The 255–316 thermolysin fragment was obtained by limited proteolysis of the 205–316 fragment with subtilisin as described elsewhere [17]. The homogeneity of the fragment, further purified by re-

* Corresponding author. Departamento de Quimica Fisica, Facultad de Ciencias, Universidad de Granada, E-18071 Granada, Spain. Fax: (34) (9) 58 274258.

SSDI 0014-5793(94)00358-3

verse phase HPLC, was at least 95%. The concentration of the 255–316 fragment was determined using the $E^{0.1\%}$ coefficient 0.52 at 280 nm [17]. Before the calorimetric experiments the sample solutions were dialyzed for 24 h at 4°C against two changes of a large volume of the dialysis buffer. For all DSC measurements sample concentrations were in the range of 0.19–4.55 mg/ml. Fragment solutions contained 0.1 M NaCl and 20 mM phosphate buffer, pH 7.5.

DSC experiments were performed in a computer-interfaced DASM-4 model [21] with 0.47-ml cells under a constant pressure of 2.5 atm. The reversibility of the transitions was checked by reheating the solution in the calorimeter cell after the first run. The scan rates used were in the range of 0.5–2.0 K/min. The excess heat capacity of the transition, $C_p^{ex}(T)$, was obtained as described in [22]. The thermograms were corrected for the effect of the time response of the instrument [23]. In calculating the molar quantities we used a molecular mass of 6,630 Da for the fragment, estimated from its known sequence. The uncertainty in the enthalpy values was between 5–10% and that of the melting temperatures, T_m, was ± 0.2°C.

3. Results and discussion

We have studied the thermal unfolding of the 255–316 fragment by DSC in 0.1 M NaCl and 20 mM phosphate buffer, pH 7.5. The process has been found to be highly reversible (> 90%) and independent of scan rate within the range 0.5–2.0 K/min, thus taking place under equilibrium conditions in the calorimeter cell. Fig. 1 shows the concentration effect of the fragment, within the range 0.19–4.55 mg/ml, on the position of the thermograms on the temperature scale. Table 1 includes the characteristic parameters of the transitions. The specific calorimetric enthalpy at the corresponding T_m values (Table 1), as well as the specific heat capacity increase of unfolding, 0.36 ± 0.08 J/K·g (0.087 ± 0.018 cal/K·g), compare well

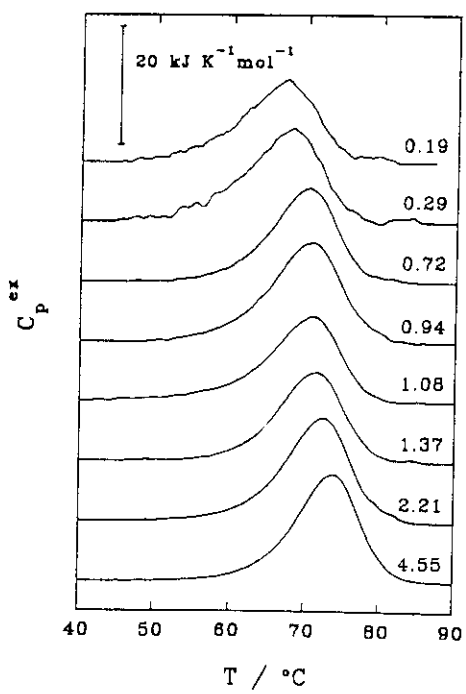

Fig. 1. Effect of sample concentration (mg/ml) on the $C_p^{ex}(T)$ curves of the 255–316 thermolysin fragment at pH 7.5. Scan rate 2.0 K/min, except for curve at 1.37 mg/ml, which is at 0.5 K/min.

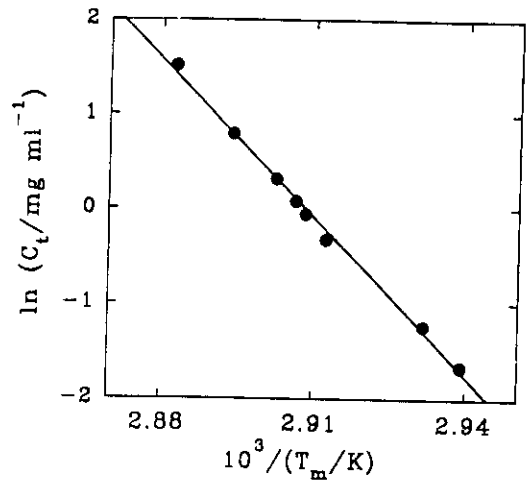

Fig. 2. Plot of ln C_t vs. $1/T_m$ for the 255–316 thermolysin fragment, pH 7.5. Values are taken from Table 1.

with values reported for compact globular proteins [19]. This shows the capacity of the 62-amino acid chain to fold into a compact globular structure.

The ratio of the calorimetric enthalpy, ΔH (obtained from the area under the calorimetric peak), to the van't Hoff enthalpy, ΔH^{vH} (obtained from the well known equation $\Delta H^{vH} = 4RT_m^2 \cdot C_p^m/\Delta H$, where C_p^m is the C_p^{ex} value at T_m), is equal to 0.55 ± 0.04 (Table 1). This value clearly suggests that the fragment undergoes dissociation upon thermal unfolding, which agrees with [18] concerning the dimeric character of the fragment within our experimental concentration range, as well as with the effect of concentration on the T_m values (Table 1).

In a general coupling between unfolding and dissociation processes, $F_n \rightleftarrows nU$, where n associated molecules of the folded fragment, F, give rise to n molecules of the unfolded fragment, U, equilibrium thermodynamics predicts the following relationship between the total fragment concentration, C_t, and the unfolding temperature, T_m [22,24],

$$\ln C_t = \text{constant} - n\Delta H/(n-1)RT_m$$

where ΔH stands for the unfolding enthalpy per monomer. The plot of ln C_t vs. $1/T_m$ (Fig. 2) for a dimer ($n = 2$) gives a straight line with a slope equal to $-2\Delta H/R$. The value of ΔH obtained from the slope is 231 ± 6 kJ/mol, close to the calorimetric enthalpy, 192 ± 13 kJ/mol (Table 1). The use of the above equation for $n > 2$ leads to much higher ΔH values.

The equation for $C_p^{ex}(T)$, which gives the shape of the thermal transitions, as reported in [15] for the unfolding of multimeric proteins, leads to excellent fittings of our experimental data for $n = 2$, whereas similar fittings for $n > 2$ were increasingly poor (Fig. 3).

Therefore, it can be concluded that the 255–316 fragment behaves as a dimer in solution, which undergoes a two-state reversible thermal unfolding under our experi-

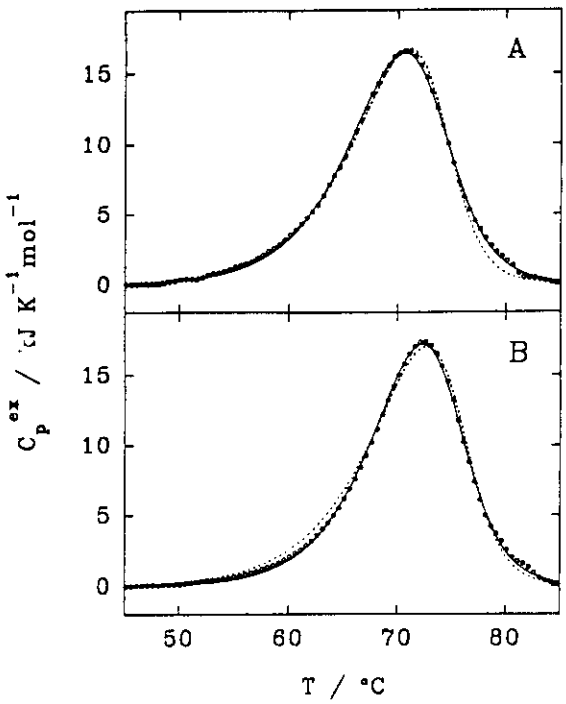

Fig. 3. Non-linear least-square fittings of the C_p^{ex} curves to the $F_n \rightleftharpoons nU$ model for the 255–316 thermolysin fragment, pH 7.5. (A) 0.94 mg/ml; (B) 2.21 mg/ml. (○) Experimental data; solid line, best fitting for $n = 2$; dotted line, best fitting for $n = 3$.

mental conditions. This dimerization agrees with previous studies [18], where an association constant at 20°C equal to $(2 \pm 1) \cdot 10^4$ M^{-1} was obtained, from which the Gibbs energy of dimerization results in -24 ± 2 kJ/mol of dimer. This is quite a large value compared to the Gibbs energy of folding of the dimer we can calculate here at 20°C from our DSC data, -60 ± 6 kJ/mol of dimer (i.e. with a dimer stability similar to that of larger globular proteins [19]). Hence, the energetics of the interactions at the contact surface between the two monomers must be particularly significant, bearing in mind the small size of the fragment.

Recently the solution structure of the dimeric fragment has been elucidated by proton NMR techniques (manuscript in preparation), where it is shown that the fragment acquires a secondary and tertiary structure very similar to that of the corresponding chain in the intact protein. Therefore, the results of all these studies decisively show that domains and subdomains in relatively large globular proteins can be viewed as independent co-operative folding units. Since thermolysin is made up of two structural domains of similar size, these studies clearly show that folding units can be substantially smaller than entire structural domains.

Table 1
Thermodynamic parameters for the DSC thermal unfolding of 255–316 thermolysin fragment at pH 7.5, different sample concentrations and scan rate 2 K/min

C_t (mg/ml)	ΔH (kJ/mol)	Δh (J/g)	ΔH^{vH} (kJ/mol)	T_m (°C)	ΔC_p (kJ/K·mol)
0.19	177	26.6	307	67.1	–
0.29	200	30.2	306	68.0	–
0.72	176	26.5	352	70.2	–
0.94	204	30.8	320	70.7	1.8
1.08	178	26.8	318	70.9	3.2
1.37[a]	170	25.6	349	71.4	2.0
2.21	199	30.0	346	72.4	2.4
4.55	199	30.0	363	73.7	2.4
Average[b]:	192 ± 13	29 ± 2	347 ± 22		2.4 ± 0.5

[a]Scan rate 0.5 K/min.
[b]Average values weighed by sample concentration.

Acknowledgements: This work was supported by Grants PB90-0876 from the DGICYT (Spain) and 0460.E from the BAP (European Union). F.C.-L. was predoctoral fellow from the DGICYT (Spain). We thank our colleague Dr. J. Trout for revising the English text.

References

[1] Wetlaufer, D.B. (1973) Proc. Natl. Acad. Sci. USA 70, 687–701.
[2] Rossmann, M.G. and Argos, D. (1981) Annu. Rev. Biochem. 50, 487–532.
[3] Janin, J. and Wodak, S.J. (1983) Prog. Biophys. Mol. Biol. 42, 21–78.
[4] Rose, G.D. (1979) J. Mol. Biol. 134, 447–470.
[5] Crippen, G.M. (1978) J. Mol. Biol. 126, 315–332.
[6] Zehfus, M.H. (1987) Proteins Struct. Funct. Genet. 2, 90–110.
[7] Wetlaufer, D.B. (1981) Adv. Prot. Chem. 34, 61–92.
[8] Holmes, M.A. and Matthews, B.W. (1982) J. Mol. Biol. 160, 623–629.
[9] Wodak, S.J. and Janin, J. (1981) Biochemistry 20, 6544–6552.
[10] Rashin, A.A. (1981) Nature 291, 85–87.
[11] Rashin, A.A. (1984) Biochemistry 23, 5518–5519.
[12] Vita, C., Fontana, A., Seeman, J.R. and Chaiken, I.M. (1979) Biochemistry 18, 3023–3031.
[13] Vita, C. and Fontana, A. (1982) Biochemistry 21, 5196–5202.
[14] Vita, C., Dalzoppo, D. and Fontana, A. (1983) Int. J. Peptide Protein Res. 21, 49–56.
[15] Fontana, A. (1990) in: Peptides: Chemistry, Structure and Biology (Rivier, J. and Marshall, G.E. Eds.) pp. 557–564. Escom, Leiden.
[16] Vita, C., Fontana, A. and Chaiken, I.M. (1985) Eur. J. Biochem. 151, 191–196.
[17] Dalzoppo, D., Vita, C. and Fontana, A. (1985) J. Mol. Biol. 182, 331–340.
[18] Vita, C., Fontana, A. and Jaenicke, R. (1989) Eur. J. Biochem. 180, 513–518.
[19] Privalov, P.L. (1979) Adv. Prot. Chem. 33, 167–241.
[20] Filimonov, V.V., Prieto, J., Martinez, J.C., Bruix, M., Mateo, P.L. and Serrano, L. (1993) Biochemistry 32, 12906–12921.
[21] Privalov, P.L. and Pothekin, S.A. (1986) Methods Enzymol. 131, 4–51.
[22] Takahashi, K. and Sturtevant, J.M. (1981) Biochemistry 20, 6185–6190.
[23] Lopez-Mayorga, O. and Freire, E. (1987) Biophys. Chem. 87, 87–96.
[24] Freire, E. (1989) Comments Mol. Cell. Biophys. 6, 123–140.

Baltimore (4-7-95)

CHAPTER 9

Differential Scanning Calorimetry

Ernesto Freire

1. Introduction

Differential scanning calorimetry (DSC) is now generally accepted as the technique of choice to determine the energetics of protein folding/unfolding transitions and the thermodynamic mechanisms underlying those reactions. Despite this fact, the theoretical framework necessary for the analysis of calorimetric data is not available to the general scientist in a comprehensive way. The purpose of this chapter is to present in a succinct form the fundamental theory of differential scanning calorimetry, to summarize the information that can be obtained with this technique, and to alert the reader of some potential problems in data interpretation.

Differential scanning calorimetry measures the apparent molar heat capacity of a protein or other macromolecule as a function of temperature. Subsequent manipulation of this quantity yields a complete thermodynamic characterization of a transition. In general, three different types of information can be obtained from DSC:

1. The absolute partial heat capacity of a molecule;
2. The overall thermodynamic parameters (enthalpy change [ΔH], entropy change [ΔS], and heat capacity change [ΔC_p]) associated with a temperature induced transition; and
3. The partition function and concomitantly the population of intermediate states and their thermodynamic parameters.

In this chapter we will restrict our discussion to monomeric protein systems undergoing reversible folding/unfolding transitions under equi-

From: *Methods in Molecular Biology, Vol. 40: Protein Stability and Folding: Theory and Practice*
Edited by: B. A. Shirley

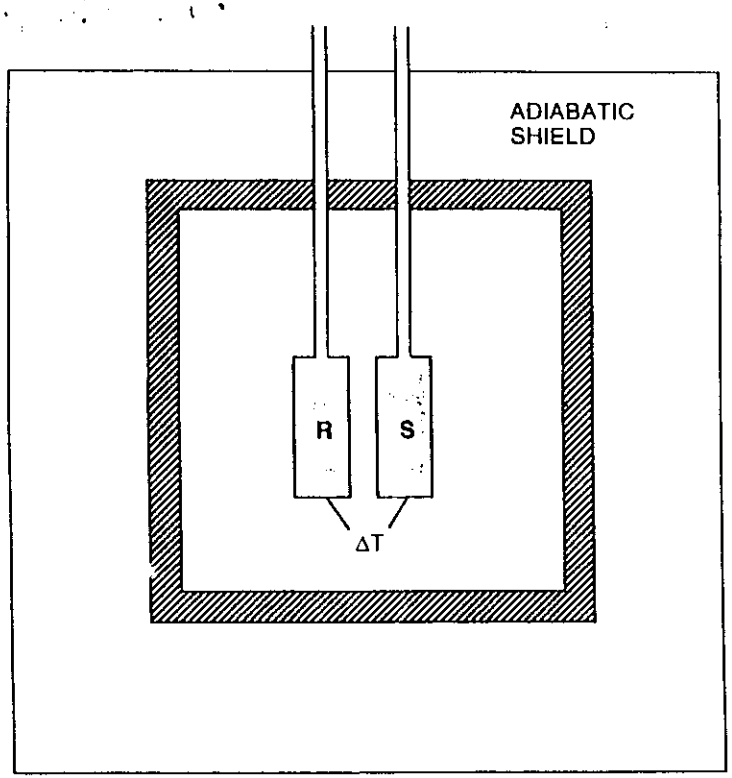

Fig. 1. Schematic illustration of the cell assembly of a differential scanning calorimeter. The temperature difference (ΔT) between the sample and reference cells (S and R) is maintained equal to zero by a feedback mechanism as the temperature is increased or decreased at a constant scanning rate. The differential power that needs to be applied to the sample cell in order to maintain $\Delta T = 0$ is monitored continuously as a function of temperature. This differential power is directly proportional to the heat capacity difference between the cells and constitutes the basic quantity measured by the instrument.

librium conditions; however, the equations and the general treatment are applicable to other macromolecular systems undergoing equilibrium monomolecular isomerization reactions.

2. Measurement

Figure 1 provides a schematic illustration of the cell compartment of a differential scanning calorimeter. It consists of two identical cells, one of

which is used to hold the sample under investigation and the other the reference solution (usually the same buffer used in the preparation of the sample solution). The two cells operate in a differential mode such that the difference in heat capacity between them is the quantity measured. This is accomplished by continuously monitoring the differential electrical power required to maintain the temperature difference between the two cells equal to zero as the temperature of the entire assembly is scanned at a constant rate. This differential electrical power (usually given in $\mu W = \mu J/s$ or in $\mu cal/s$) after normalization by the scanning rate yields the difference in heat capacity between the two cells (units of $\mu J/deg$ or $\mu cal/deg$). Ideally, if the two cells were identical, a single scan would be enough to determine the difference in heat capacity between the sample and the reference solution. In practice, however, the two cells are never perfectly matched and two separate scans are required in order to subtract and eliminate instrumental effects.

A properly performed calorimetric experiment consists of a minimum of three runs: a buffer scan and two scans of the sample under study. The second scan of the sample is normally used to assess the reversibility of the transition. Usually, the reversibility is expressed in terms of the percentage of the original signal that is recovered in the second scan. This is an important check since an analysis based on equilibrium thermodynamics *cannot* be applied to a sample that undergoes an irreversible transition. Protein samples for calorimetric measurements need to be prepared following very rigorous and exact procedures that guarantee the purity and integrity of the protein under study. Protein concentrations must be determined with high accuracy since any error in concentration will be reflected directly in the measured thermodynamic parameters. For example, a 5% error in concentration will introduce a 5% error in the measured enthalpy change. Samples for calorimetric analysis must be dialyzed against the desired buffer, centrifuged to remove aggregates and dust particles, and degassed. The protein concentration must be measured after all sample preparation steps have been performed and the sample is ready to load in the calorimeter cell. The degassed buffer used in the final dialysis during sample preparation must be loaded into the reference cell of the instrument in order to insure that the solvents in the two cells are identical. This is especially critical if absolute values of the apparent heat capacities are needed

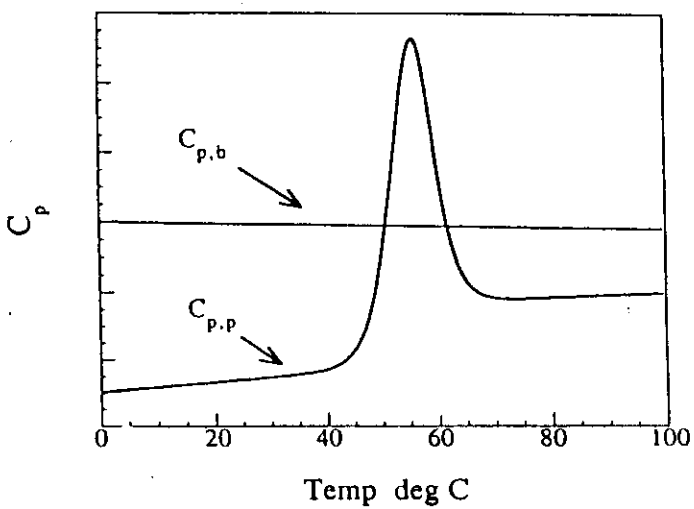

Fig. 2. Schematic representation of a typical calorimetric scan of a globular protein. The heat capacity of the protein solution ($C_{p,p}$) displays the characteristic peak associated with the unfolding transition. The heat capacity of the buffer solution ($C_{p,b}$) is higher than that of the protein solution. The partial heat capacity of globular proteins in the native state is on the order of 0.3 cal/K/g at 20°C *(1)*.

Figure 2 illustrates a typical set of results for a globular protein. The quantity obtained from a calorimetric scan is the heat capacity of the solution present in the calorimeter cell. In order to determine the heat capacity of the protein, the data from the protein solution scan and the buffer scan are needed. For the buffer (solvent) scan the measured heat capacity can be written as:

$$C_{p,b} = m_b \cdot C_{p,b}^o \tag{1}$$

where m_b is the mass of solvent in the cell and $C_{p,b}^o$ is the specific heat capacity of the buffer solution. Similarly, the heat capacity of the protein solution can be written as:

$$C_{p,p} = m_p \cdot C_{p,p}^o + m_b' \cdot C_{p,b}^o \tag{2}$$

where $C_{p,p}^o$ is the heat capacity of the protein per unit mass, m_p is the mass of protein in the calorimetric cell, and m_b' is the mass of solvent. $C_{p,p}^o$ can be obtained as follows:

$$C_{p,p}^o = [(C_{p,p} - C_{p,b}) + (m_b - m_b') \cdot C_{p,b}^o] / m_p \tag{3}$$

The quantity $(m_b - m_b')$ is equal to the mass of solvent displaced by the protein and can be written in terms of the partial specific volume of the protein as Eq. (1):

$$C_{p,p}^o = (C_{p,p} - C_{p,b})/m_p + C_{p,b}^o \cdot (V_p^o/V_b^o) \tag{4}$$

where V_p^o and V_b^o are the partial specific volumes of the protein and solvent, respectively. The molar heat capacity function (C_p) is simply equal to $C_{p,p}^o$ multiplied by the molecular weight of the protein. C_p is the main quantity measured by DSC and constitutes the center of our discussion.

3. Absolute Heat Capacity of Proteins

In the past, most analyses of DSC data were aimed at obtaining transition-related thermodynamic parameters. It was realized recently, however, that the absolute values of $C_{p,p}^o$ and C_p also contain fundamental information regarding the structural state of a protein. For example, it has been shown that the heat capacity of a protein in the unfolded state ($C_{p,u}$) can be calculated with high accuracy from the amino acid sequence *(2)*. If all the constituent groups are exposed to water, then $C_{p,u}$ obeys simple additivity rules and can be expressed in terms of the individual contributions from the amino acid side chains and the peptide backbone:

$$C_{p,u} = \left(\sum_{i=1}^{20} n_i \cdot C_{p,i}\right) + (N_{AA} - 1) \cdot C_{p,bb} + C_{p,\mathrm{NH2}} + C_{p,\mathrm{COOH}} \tag{5}$$

where the index in the summation refers to the 20 amino acids, n_i is the number of amino acids of type i and $C_{p,i}$ the molar heat capacity of its side chain; N_{AA} is the number of amino acids in the protein; $C_{p,bb}$ is the heat capacity of a peptide backbone unit (-CHCONH-), $C_{p,\mathrm{NH2}}$ the heat capacity of the amino terminus, and $C_{p,\mathrm{COOH}}$ the heat capacity of the carboxy terminus. Table 1 summarizes the parameters necessary to estimate $C_{p,u}$ from the amino acid sequence of a protein. The parameters in Table 1 were obtained by a polynomial fit of the data published by Privalov and Makhatadze *(2)* (Freire and Muphy, unpublished results).

The heat capacity of a protein in the native state ($C_{p,n}$) has been shown to be a linear function of temperature *(2)* within the range in which it can be measured (i.e., the temperature range in which the native state constitutes over 99% of the total population). Within that range the heat capacity of the native state is very similar for all proteins when normalized on a weight basis. Therefore, the molar heat capacity can be written as

Table 1
Heat Capacity of Proteins in Unfolded State[a]

Amino acid	A	B	C	D
A. Side chain contributions				
ALA	177.957	–0.450	0.000153	
ARG	299.558	0.627	–0.00267	
ASN	68.395	0.884	–0.00160	
ASP	68.731	0.8206	–0.00107	
CYS	222.58	0.636	–0.0017	
GLN	165.183	0.6360	–0.0017	
GLU	164.742	0.636	–0.00168	
GLY	83.505	–0.226	-9.54×10^{-05}	
HIS	212.367	–1.699	0.0230	-8.36×10^{-05}
ILE	408.045	–0.233	0.000115	
LEU	386.787	–0.198	0.000225	
LYS	316.945	–1.365	0.0188	-7.434×10^{-05}
MET	200.523	–1.0456	0.00487	
PHE	398.560	–0.6340	0.00130	
PRO	218.452	–1.623	0.0075	
SER	74.736	0.233	–0.000108	
THR	196.165	–0.571	0.00589	
TRP	474.060	–0.634	0.00130	
TYR	314.312	–0.716	0.00785	-2.2×10^{-05}
VAL	325.226	–0.361	–0.000586	
B. Peptide backbone unit contribution (-CHCONH-)				
	1.273	0.613	–0.00286	
C. Amino terminal contribution (NH2)				
	–192.630	6.178	–0.0666	0.000157
D. Carboxy terminal contributions (COOH)				
	1.273	0.613	–0.00286	

[a]The coefficients were obtained by a polynomial least squares fit of the data published by Privalov and Makhatadze *(2)* (Freire and Murphy, unpublished results). $C_{p,u}(T) = A + BxT + CxT^2 + DxT^3$ where C_p is in J/K/mol and T in °C.

$$C_{p,n} = (a_N + b_N \cdot T) \cdot M_r \quad (6)$$

where $a_N = 0.3161 \pm 0.013$ cal/K · g, $b_N = 0.0016 \pm 0.0003$ cal/K^2 · g, and M_r is the molecular weight of the protein.

Recently, it has been shown that the heat capacity difference (ΔC_p) between the unfolded and native states is directly proportional to the change in solvent accessible polar and apolar surfaces between those states *(3,4)*:

$$\Delta C_p = \Delta C^\circ_{p,ap} \cdot \Delta A_{ap} + \Delta C^\circ_{p,pol} \cdot \Delta A_{pol} \quad (7)$$

where $C^\circ_{p,ap}$ (0.45 ± 0.02 cal/K/[mol-Å^2]) and $C^\circ_{p,pol}$ (–0.26 ± 0.03 cal/K/[mol-Å^2]) are the elementary apolar and polar contributions to the total heat capacity increment; and ΔA_{ap} and ΔA_{pol} are the differences between the solvent accessible apolar and polar surface areas of the two states. The above approach accurately predicts the heat capacity values obtained for the native state of globular proteins and the magnitude of the heat capacity change associated with the complete unfolding of the protein. The heat capacity values provide a means to evaluate the degree of unfolding of a protein by comparing experimentally determined values to those calculated with Eqs. (5), (6), and (7). In conjunction with the measured changes in ΔH and ΔS on unfolding, the heat capacity values provide a rather complete assessment of the degree of unfolding of a protein.

Because of the curvature of $C_{p,u}$ and the linearity of $C_{p,n}$, ΔC_p decreases at higher temperatures. This decrease is, however, small within the temperature range of interest. For example, in most cases in which the temperature dependence of the enthalpy change has been measured over a wide temperature interval, no evidence of a diminished slope at high temperatures has been observed *(7)*. For practical purposes, the enthalpy change within the temperature range 0–80°C can be accounted for with a constant ΔC_p.

4. Excess Heat Capacity Function

DSC has been utilized primarily to study thermally induced structural transitions *(8)*. If a protein undergoes a transition, the heat capacity function will exhibit an anomaly at some characteristic temperature, usually called the transition temperature *(T_m)*. Under these conditions, the heat capacity function can no longer be ascribed to a single structural state since it contains contributions from all the states that become populated during the transition as well as the excess contributions arising from the existence of enhanced enthalpy fluctuations within the temperature transition region. These excess contributions give rise to the characteristic peak or peaks associated with thermally induced transitions *(9,10)*. The most important quantity for the thermodynamic analysis of the thermal unfolding of a protein is the excess heat capacity function ($<\Delta C_p>$) that is obtained by subtracting the heat capacity of the native state from the measured heat capacity function *(11)*:

$$<\Delta C_p> = C_p - C_{p,n} \quad (8)$$

Figures 3 and 4 illustrate the procedure required to estimate $<\Delta C_p>$ from the experimental data

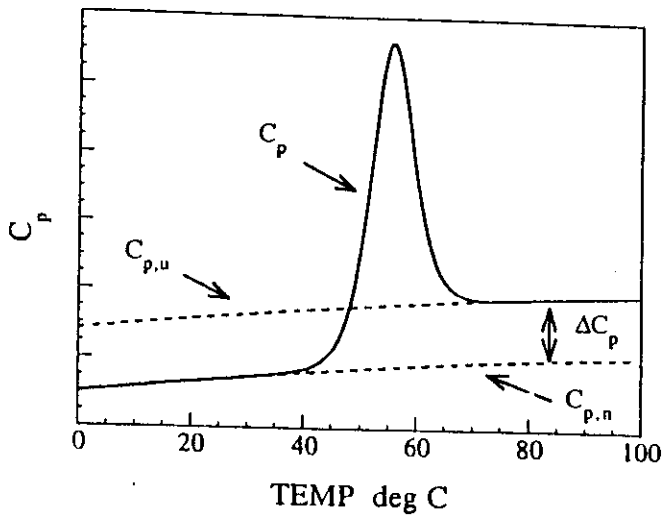

Fig. 3. The molar heat capacity function (C_p) obtained by Eq. (4). The molar heat capacities of the unfolded ($C_{p,u}$) and native ($C_{p,n}$) states are indicated by the dashed lines. The difference between these values define the heat capacity change for the transition ($\Delta C_p = C_{p,u} - C_{p,n}$).

extrapolation of $C_{p,n}$ to those temperature regions in which the native state is no longer the most significantly populated. This extrapolation might introduce systematic distortions in $<\Delta C_p>$ and therefore must be done with extreme care. Potential extrapolation errors can be minimized by:

1. Measuring a relatively long pretransition baseline so that its mathematical form can be determined; and
2. Performing several calorimetric scans under conditions in which the transition occurs at different temperatures and $C_{p,n}$ can be defined over a wider temperature range. The subtraction of $C_{p,n}$ from $<C_p>$ implicitly selects the native state as the reference state.

5. Statistical Thermodynamic Definition of the Excess Heat Capacity Function

In the analysis of DSC data, the most important quantity that needs to be defined using the tools of statistical thermodynamics is the average excess enthalpy function ($<\Delta H>$). This quantity is the sum of the enthalpy contributions of all the states that become populated during the transition *(11)*:

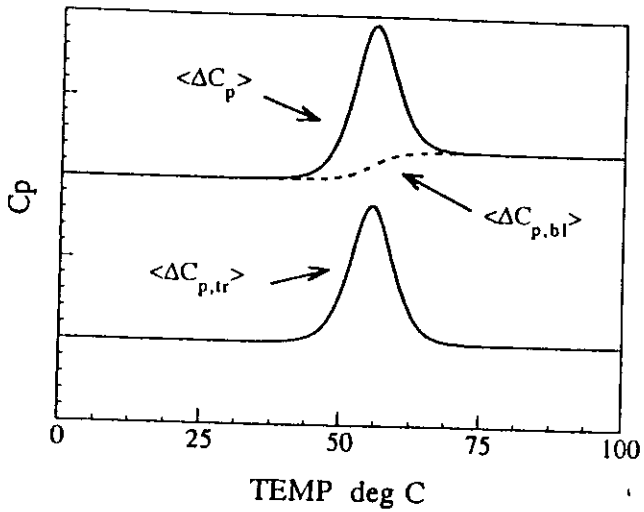

Fig. 4. The excess heat capacity function ($<\Delta C_p>$) is obtained by subtracting the molar heat capacity of the native state ($C_{p,n}$) from the molar heat capacity of the protein (C_p). $<\Delta C_p>$ is composed of two contributions: the transition excess heat capacity function ($<\Delta C_{p,tr}>$) and the sigmoidal function ($<\Delta C_{p,bl}>$) that gives rise to the baseline shift characteristic of transitions accompanied by a positive ΔC_p.

$$<\Delta H> = \sum_{i=0}^{N} P_i \cdot \Delta H_i \tag{9}$$

where P_i represents the population or probability of state i, and ΔH_i the enthalpy of the i^{th} state relative to that of the native state that is taken as the reference state. $<\Delta C_p>$ is equal to the temperature derivative of $<\Delta H>$ at constant pressure:

$$<\Delta C_p> = \sum_{i=1}^{N} \Delta H_i \cdot (\partial P_i/\partial T) + \sum_{i=1}^{N} P_i \cdot \Delta C_{p,i} \tag{10a}$$

$$= <\Delta C_{p,tr}> + <\Delta_{Cp,bl}> \tag{10b}$$

The first term on the right hand side ($<\Delta C_{p,tr}>$) is the *transition excess heat capacity function* and defines the characteristic transition peak(s) in the heat capacity function (Fig. 4) *(12)*. The second term on the right hand side ($<\Delta C_{p,bl}>$) defines the "S-shape" shift in baseline usually asso-

ciated with protein unfolding or other transitions characterized by positive changes in ΔC_p *(12)*.

$<\Delta H>$ is the cumulative integral of $<\Delta C_p>$:

$$<\Delta H> = \int_{T_o}^{T} <\Delta C_p> \, dT \tag{11}$$

where T_o is a temperature in which the protein is in the native state (Fig. 4). Eqs. (9) and (10) are functions of the population of molecules in the different states accessible to the protein molecule. The population of molecules in state j (P_j) is equal to:

$$P_j = \exp(-\Delta G_j/RT)/[1 + \sum_{i=1}^{N} \exp(-\Delta G_i/RT)] \tag{12}$$

where $\Delta G_j = \Delta H_j - T \cdot \Delta S_j$ is the Gibbs free energy difference between state j and the native state (state *0*) and R the gas constant. The quantity in the denominator in Eq. (12) is the folding/unfolding partition function Q defined as:

$$Q = 1 + \sum_{i=1}^{N} \exp(-\Delta G_i/RT) \tag{13}$$

The partition function contains all the thermodynamic information of the system and is therefore sufficient to describe the thermal unfolding of a protein. It must noted that the above statistical thermodynamic treatment requires no *a priori* assumptions regarding the number of states or the magnitude of the thermodynamic parameters associated with the folding/unfolding equilibrium.

For convenience, Eq. (13) can be written as:

$$Q = 1 + \sum_{i=1}^{N-1} \exp(-\Delta G_i/RT) + \exp(-\Delta G_N/RT) \tag{14}$$

where the terms under the summation include all intermediates that become populated during the transition. The first and last terms are the statistical weights of the native and unfolded states respectively. For a two-state transition the partition function reduces to $Q = 1 + \exp(-\Delta G_N/RT)$.

6. Overall Thermodynamic Parameters

The most important overall thermodynamic parameters associated with the thermal unfolding of proteins are the enthalpy (ΔH), entropy

(ΔS), and heat capacity (ΔC_p) changes between the unfolded and native states. The free energy change is defined in terms of ΔH, ΔS, and ΔC_p using the standard equation:

$$\Delta G(T) = \Delta H(T_R) + \int \Delta C_p dT - T[\Delta S(T_R) + \int \Delta C_p d\ln T] \tag{15a}$$

$$\Delta G(T) = \Delta H(T_R) + \Delta C_p \cdot (T - T_R) - T \cdot [\Delta S(T_R) + \Delta C_p \cdot \ln(T/T_R)] \tag{15b}$$

where Eq. (15b) is the classical equation for the case in which ΔC_p is temperature independent.

All these parameters are state functions, i.e., their value only depends on the nature of the unfolded and the native states and not on the specific transition pathway or the presence of partly folded intermediates. From a practical point of view, these parameters are independent of the shape of the measured heat capacity function. The heat capacity change is defined by the value of $<\Delta C_p>$ after completion of the transition, as indicated in Fig. 4. The enthalpy change is the area under the transition excess heat capacity function ($<\Delta C_{p,tr}>$):

$$\Delta H = \int_{T_o}^{T_f} <\Delta C_{p,tr}> \, dT \tag{16}$$

where the limits of integration are defined by the onset and completion temperatures of the transition (i.e., the temperatures at which essentially all molecules are in the initial and final states, respectively). The entropy change is simply evaluated by means of:

$$\Delta S = \int_{T_o}^{T_f} <\Delta C_{p,tr}> \, d\ln T \tag{17}$$

Both ΔH and ΔS, as defined by Eqs. (16) and (17), are referred to the transition temperature, T_m, i.e., $\Delta H = \Delta H(T_m)$ and $\Delta S = \Delta S(T_m)$. It must be noted that Eqs. (16) and (17) are defined in terms of the *transition* excess heat capacity curve, implying that $<\Delta C_{p,bl}>$ needs to be subtracted from the excess heat capacity function. Throughout the years, different subtraction methods have been utilized. In the past, $<\Delta C_{p,bl}>$ used to be approximated by a step function defined by the intersection of a vertical line centered at T_m with the extrapolated initial and final values of the

heat capacity function (*see*, for example refs. *6,8*). Since the baseline is proportional to the degree of unfolding (*see* Eq. [10]) a more accurate way of estimating it can be achieved by defining its shape in terms of the normalized integral of the heat capacity function *(13,14)*. This alternative is easy to implement with computer digitized data and is mathematically exact for a two-state transition. In general, the overall thermodynamic parameters ΔH and ΔS are relatively insensitive to the exact method used to subtract $\langle \Delta C_{p,bl} \rangle$ *(15)*. The situation is different, however, for the analysis of the shape of the heat capacity function.

7. Experimental Evaluation of the Partition Function

As indicated above, the excess enthalpy function plays a central role in the statistical thermodynamic analysis of DSC data because it provides a direct link between the experiment and the folding/unfolding partition function. $\langle \Delta H \rangle$ can be calculated in terms of the cumulative integral of the measured $\langle \Delta C_p \rangle$ and is also related to the partition function by the equation:

$$\langle \Delta H \rangle = RT^2(\partial \ln Q/\partial T) \tag{18}$$

Freire and Biltonen *(11)* first realized that, by rewriting Eq. (18) in integral form, DSC could provide a direct numerical access to the folding/unfolding partition function:

$$\ln Q = \int_{T_o}^{T} \langle \Delta H \rangle / RT^2 dT \tag{19a}$$

$$\ln Q = \int_{T_o}^{T} 1/RT^2 \left(\int_{T_o}^{T} \langle \Delta C_p \rangle dT \right) dT \tag{19b}$$

The above equations provide a rigorous foundation to the deconvolution theory of the excess heat capacity function, since they establish a mathematical linkage between the experimental data and the most fundamental function in statistical thermodynamics. The uniqueness of the enthalpy function as a physical observable can be illustrated by comparing it with the observables measured by other techniques. The measured value of any arbitrary physical observable used to monitor a thermal transition can be written in terms of an equation similar to the one derived for the excess enthalpy function (Eq. [9]):

$$\langle \alpha \rangle = \sum_{i=0}^{N} \alpha_i \cdot P_i \tag{20}$$

where $\langle \alpha \rangle$ is the measured value of the observable and α_i is the characteristic value of the observable for the i^{th} state. The key feature that distinguishes the excess enthalpy function from any other physical observable is that the population of each state (P_i) is a function of its enthalpy (ΔH_i) as seen in Eq. (12). This unique feature of DSC data has made possible the development of rigorous deconvolution algorithms aimed at obtaining a complete thermodynamic characterization of a folding/unfolding transition. For other physical observables the characteristic α_i values are not mathematically related to the P_i values, i.e., the amplitude of the melting curves are not related to a thermodynamic function, and the experimental data cannot be used to obtain a complete thermodynamic description of a transition.

8. Deconvolution of the Excess Heat Capacity Function

The main goal of the deconvolution analysis of the heat capacity function is the determination of the number of states that become populated during thermal unfolding and the thermodynamic parameters for each of those states. Throughout the years the deconvolution algorithms have been perfected in different ways (*see*, for example, *11,15–17*). Nowadays, the most effective algorithms involve a recursive deconvolution procedure that includes multiple cycling through each individual transition step combined with nonlinear least squares optimization, and conclude with a global nonlinear least squares optimization. A recent example can be found in the analysis of the multistate transition of the molecular chaperone DnaK *(17)*. Figure 5 illustrates some of the results obtained for this protein.

In performing a deconvolution analysis, special attention must be paid to the following points:

1. *Calculation of excess heat capacity function.* $\langle \Delta C_p \rangle$ is obtained by subtracting the heat capacity of the initial state from the molar heat capacity function (C_p). It is important that at the initial temperature for integration essentially all molecules are in the native state, otherwise a substantial error will be introduced in all thermodynamic parameters *(12)*.
2. *General strategy.* The nonlinear least squares fit of $\langle \Delta C_p \rangle$ must be per-

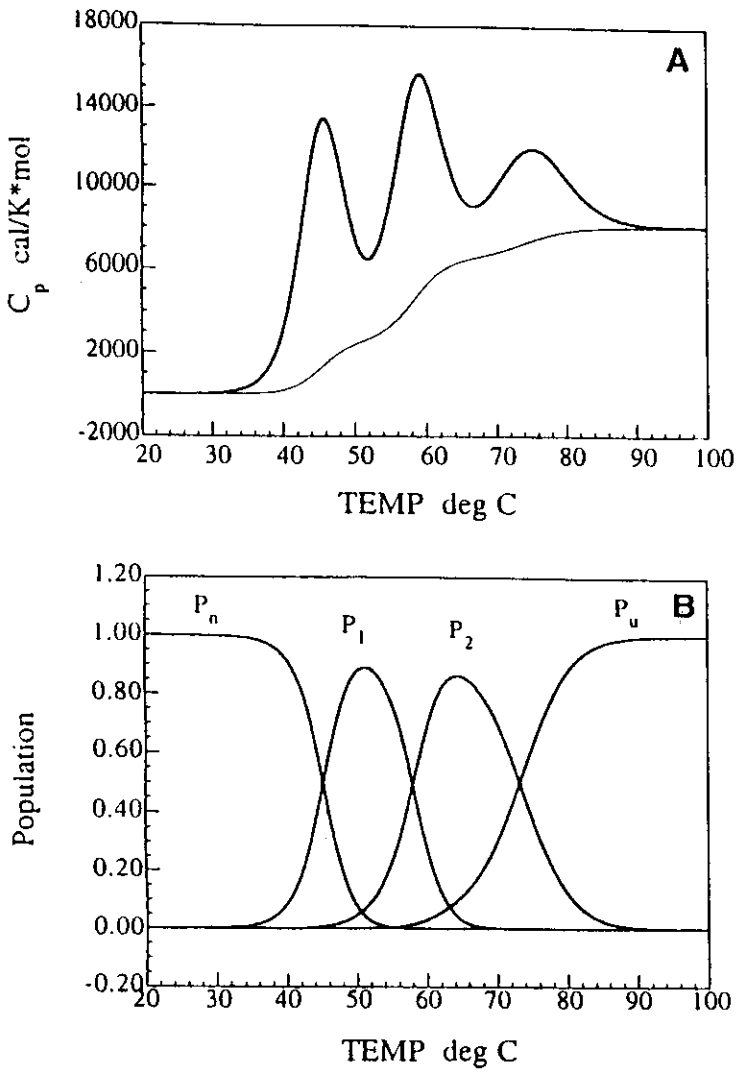

Fig. 5. The excess heat capacity function for the molecular chaperone DnaK obtained at pH 7.6 25 m*M* phosphate buffer (**A**) and the population of states resulting from the deconvolution of the heat capacity function (**B**). The thermal unfolding of this protein involves four states, each of which is characterized by enthalpy, entropy, and heat capacity changes. All the thermodynamic parameters could be obtained by deconvoluting the heat capacity function as described by ref. *17*.

formed using Eq. 10, which is the exact equation for a folding/unfolding transition exhibiting an arbitrary number of states. After convergence, the nonlinear least squares procedure returns the best set of parameters that minimizes the sum of squared residuals (SSR) between the calculated and experimental values (SSR = $\sum$ ($<\Delta C_p>_{calculated} - <\Delta C_p>_{experimental})^2$. The analysis must begin by assuming the simplest situation, i.e., the two-state case, and progressively increase the number of states. After completion of the nonlinear least squares optimization the quality of the fit must be evaluated in terms of the standard deviation of the fit and by performing an analysis of residuals *(18)*. Since there are three extra fitting parameters (ΔH, ΔS, ΔC_p) for each additional state included in the analysis, it is expected that the quality of the fit will increase with the number of states. It is necessary, then, to evaluate whether the increase in the quality of the fit actually reflects the existence of an additional state or is merely owing to the larger number of parameters used in the analysis. This can be done by performing an F-test statistics as described by ref. *18*.

3. *Estimation of initial parameter values.* In principle, initial parameter estimation can be performed in different ways: by visual inspection of the data; automatically with the deconvolution algorithm; or interactively by a combination of visual inspection of the data and a simulation program. In general, the most accurate methods are those that involve the recursive deconvolution algorithms since they yield parameter estimates that are already close to the final convergence values. This is especially true for strongly overlapped transitions. Also, it is important to check that the minimum in SSR is produced by a unique set of parameter values. Otherwise the system might exhibit multiple minima and not a unique solution.
4. *Variational analysis of baseline estimate.* In theory, the subtraction of the heat capacity of the initial state, $C_{p,n}$, can be incorporated into the nonlinear least squares algorithm. However, this practice is dangerous, especially if the variation in $C_{p,n}$ is left unrestrained. A better alternative is to perform a variational analysis in which $C_{p,n}$ is varied, within experimental confidence limits, after each cycle of nonlinear least squares optimization of the thermodynamic parameters. This procedure allows selection of the best baseline-parameter set combination.
5. *Error estimation of fitting parameters.* A convenient method to estimate joint confidence intervals for the fitted parameters involves the use of a nonlinear support plane method *(12,19,20)*. To estimate the confidence interval for a fitted parameter, that parameter is fixed at selected points around the convergence value and all other parameters are allowed to float. Then, the resulting variance of the fit is plotted as a function of the values

of the fixed parameter in order to evaluate the minimum of this function. A sharp minimum is indicative of a well defined and robust parameter estimation, whereas a shallow minimum or multiple minima are indicative of considerable uncertainty in the estimated parameter value.

It must be noted that the above analysis only includes the errors owing the optimization procedure. Errors owing to protein concentration ncertainties, baseline subtraction, and so on, must be considered sepately and added to the above error estimates. In general, it is a good idea repeat the nonlinear least squares optimization for several baseline btractions and for concentration values that bracket the limits of the perimental uncertainty.

9. van't Hoff Analysis

The deconvolution approach for characterizing folding/unfolding nsitions of proteins is far superior than the classical approach based the evaluation of the $\Delta H_{vh}/\Delta H$ ratio. In the past, the two state charac- of a folding/unfolding transition was inferred from the equality of the n't Hoff and calorimetric enthalpies. Usually, the van't Hoff enthalpy calculated by means of the formula *(1)*:

$$\Delta H_{vh} = 4 \cdot R \cdot T_m^2 \cdot <\Delta C_{p,tr}>_{max}/\Delta H \qquad (21)$$

hich utilizes a single temperature point from the entire heat capacity nction to perform the calculation. For this reason the resulting value is very sensitive to deviations that occur away from the temperature ation of $<\Delta C_{p,tr}>_{max}$. In many cases the population of partly folded ermediates is not very large and as such it can be easily missed by a mple van't Hoff analysis. This situation can be illustrated with the mple given in Fig. 6. In that figure, the excess heat capacity function the population of states associated with a hypothetical three-state nsition have been plotted as a function of temperature. As indicated in figure, the population of the partly folded intermediate reaches a ximum of 25% within the transition region even though the $\Delta H_{vh}/\Delta H$ o is 0.9. This $\Delta H_{vh}/\Delta H$ ratio is within the range obtained by Privalov *8)* for several globular proteins. If experimental uncertainties are luded, this transition would have been mistakenly characterized as a -state transition.

Figure 6 also show the result obtained by applying the deconvolution equation:

$$d \ln(Q - 1)/dT = \Delta H_1 + <\Delta H_1> \qquad (22)$$

o the hypothetical data. In that equation ΔH_1 is the enthalpy difference between the first intermediate and the native state, and $<\Delta H_1>$ is the average excess enthalpy function that would exist if the first intermediate were the lowest enthalpy state and the native state did not exist *(11)*. As seen in the figure, application of the first recursive deconvolution equation clearly indicates the existence of an intermediate state.

The above example highlights the need for a more exhaustive analysis of the heat capacity function than that provided by a simple van't Hoff analysis. This is especially true now that it is known that not all small globular proteins undergo two-state folding/unfolding transitions and that, under certain solvent conditions, many globular proteins exhibit a significant population of intermediates *(21–24)*.

Another common situation that leads to anomalous $\Delta H_{vh}/\Delta H$ ratios occurs when the transition temperature of the protein under study is low and the onset of cold denaturation occurs before the native state is fully populated. Under those conditions ΔH is underestimated, ΔH_{vh} is overestimated, and therefore a $\Delta H_{vh}/\Delta H$ ratio >1 is observed even for two-state transitions. This situation was observed by Xie et al. *(22)* in their analysis of apo α-lactalbumin and has been discussed in detail by Straume and Freire *(12)*. In those cases, a straightforward interpretation of the $\Delta H_{vh}/\Delta H$ ratio yields a wrong assessment of the transition. In the case of apo α-lactalbumin, for example, a $\Delta H_{vh}/\Delta H$ ratio >1 is observed in the presence of moderate GuHCl concentrations even though the transition is characterized by the presence of a partly folded intermediate. In general, a single calorimetric curve obtained under such conditions cannot be analyzed correctly unless the heat capacity of the native state is known accurately. If this information is not available, a rigorous analysis can still be performed by introducing a second independent variable (e.g., pH, ligand concentration, and so on) and implementing a two-dimensional analysis of the data (*see* Section 11).

10. Heat and Cold Denaturation

As mentioned above, the unfolding of a protein is accompanied by a positive ΔC_p. As a result, both the enthalpy and entropy changes are

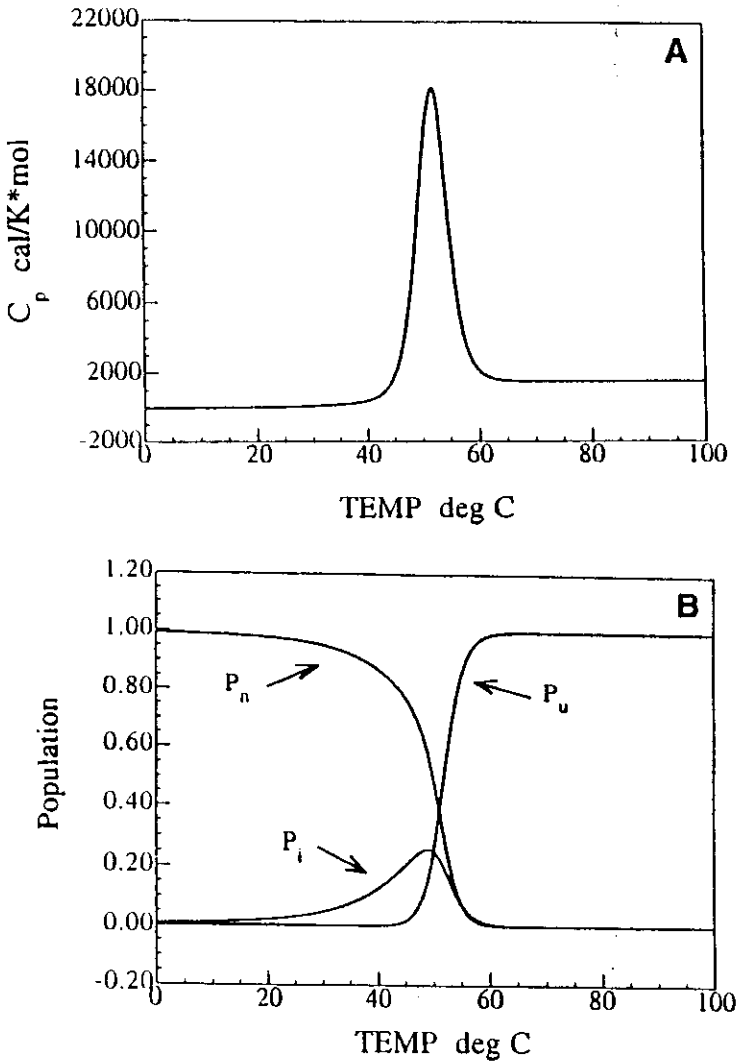

Fig. 6. (A) Simulated heat capacity function associated with a hypothetical three state transition characterized by the following parameters: $\Delta H_1(T_{m1}) = 30$ kcal/mol; $T_{m1} = 55°C$; $\Delta C_{p2} = 500$ cal/K/mol; $\Delta H_2(T_{m2}) = 100$ kcal/mol; $T_{m2} = 50°C$; $\Delta C_{p2} = 1000$ cal/K/mol. (B) As shown in this figure, the maximal population of the intermediate is close to 25% within the transition region. As explained in the text, the $\Delta H_{vh}/\Delta H$ is very close to one, implying that with that simplistic analysis this transition can be mistakenly characterized as a two-state transition, even though the intermediate population is significant.

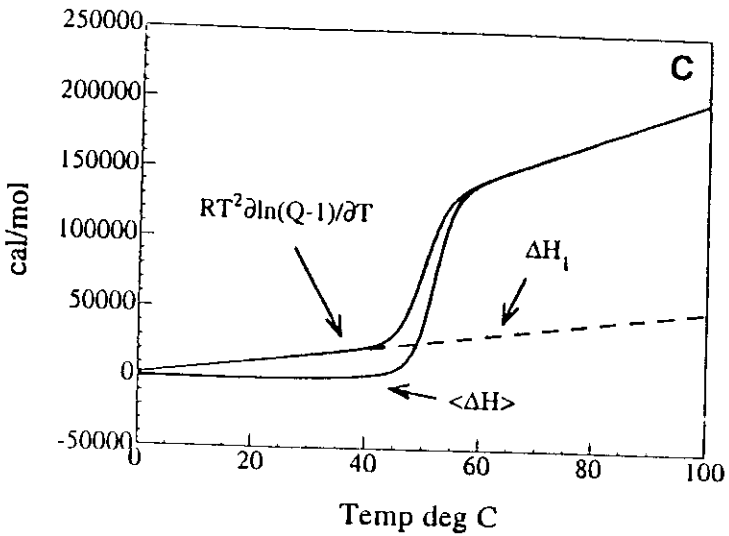

(C) A plot of the excess enthalpy function and the first recursive deconvolution function reveals a significant difference between them and illustrates the enthalpy change for the first intermediate.

increasing functions of temperature. The resulting Gibbs free energy function, on the other hand, exhibits a maximum at a characteristic temperature called the *temperature of maximal stability*. This temperature occurs at the point in which the entropy change is zero. Heating above this temperature or cooling below this temperature destabilizes the protein. This situation is illustrated in Fig. 7 for a typical globular protein. As shown in the figure, there are two temperatures at which the Gibbs free energy function is zero. These temperatures correspond to the temperature of cold and heat denaturation, respectively.

Most of the thermodynamic data for globular proteins have been obtained by performing DSC scans as a function of pH under conditions in which the enthalpic contributions owing to ionization are negligible *(1)*. Under those conditions the observed changes in protein stability are primarily entropic in origin. This situation is also illustrated in Fig. 7. It must be noted that, as the stability of the protein decreases, a point is reached in which ΔG is negative at all temperatures. Under those conditions, the system still exhibits a peak in a calorimetric scan, however the location of that peak cannot be interpreted as the temperature at which

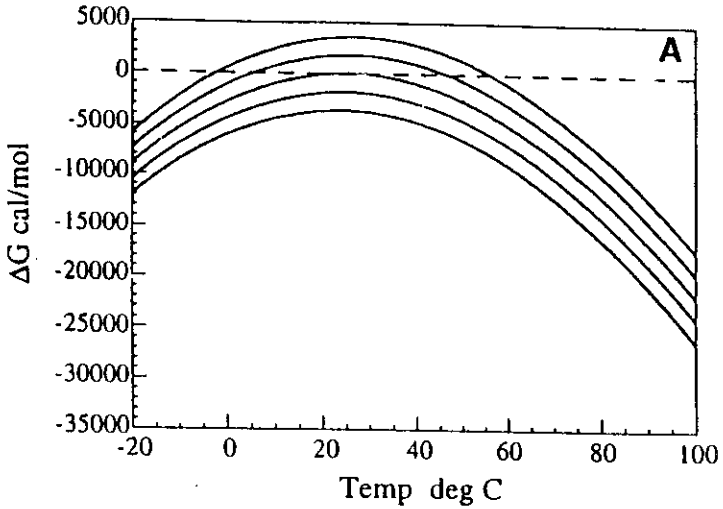

Fig. 7. (A) Gibbs' free energy (ΔG) vs temperature for a transition characterized by the following thermodynamic parameters: ΔC_p = 2500 cal/K/mol, $\Delta H(25) = 0$, and, from top to bottom $\Delta S(25) = -12, -6, 0, 6, 12$ cal/K/mol. It must be noted that as a protein is destabilized, a point is reached in which ΔG is never greater than zero. Formally, there is no transition temperature, even though transition peaks will still be observed in calorimetric scans. A conventional analysis of peaks obtained under destabilizing conditions will lead to substantial errors in the thermodynamic parameters.

$G = 0$ since that temperature does not exist. Of course, a conventional baseline subtraction yields an artificially low ΔH and an artificially high H_{vh} as explained above. Further destabilization of the protein accentues this trend and eventually leads to the absence of a transition, a situation that should not be interpreted as indicating that the native and denatured states are enthalpically equivalent. Because of the existence of positive ΔC_p between the unfolded and native states there is a temperature at which $\Delta H = 0$ (sometimes called the *inversion* temperature), however, ΔH is different than zero at all other temperatures independently of whether a transition is observed or not.

The situation illustrated in Fig. 7 also highlights the need for a more rigorous analysis than that provided by conventional baseline subtraction followed by a van't Hoff analysis. In fact, we recommend that decisions about the two-state or multistate character of a transi[illegible] not be made on the basis of the value of the $\Delta H_{vh}/\Delta H$ ratio. Shrake and Ross *(25)* have also pointed out other situations in which the $\Delta H_{vh}/\Delta H$ ratio is different than one even for two-state transitions. Similarly, a $\Delta H_{vh}/\Delta H$ ratio of unity should not be interpreted as sufficient proof that a transition conforms to the two-state model.

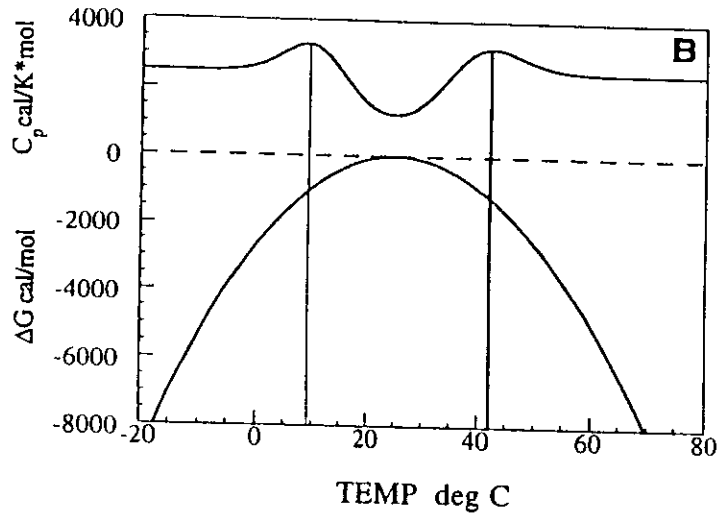

(B) Plot of ΔG and the heat capacity function for the case in which $\Delta S(25) = 0$. As seen in the figure, under those conditions the temperature location of the peaks in the heat capacity function do not correspond to the temperatures at which $\Delta G = 0$.

11. Two-Dimensional Differential Scanning Calorimetry

The examples discussed in the previous section illustrate the dangers of performing a conventional van't Hoff analysis on protein folding/unfolding transitions characterized by very low transition temperatures. Under those conditions a rigorous alternative is to perform a two-dimensional analysis of the excess heat capacity function. A heat capacity surface is obtained by performing calorimetric scans as a function of a second variable. The resulting surface is then analyzed in terms of the linkage equations between the two variables. We will use pH as an example of a second variable but the equations can be easily generalized to other cases of ligand bi[illegible]ng *(12)* or to the effects of denaturants *(13,22)*.

The folding/unfolding partition function including protonation effects can be written as:

$$Q = 1 + \sum_{i=1}^{N-1} [\exp(-\Delta G_i^o/RT) \cdot \prod_{j=1}^{m} (1 + K_{ij} \cdot a_H)/(1 + K_{nj} \cdot a_H)]$$

$$+ \exp(-\Delta G_N^o/RT) \cdot \prod_{j=1}^{m} (1 + K_{Nj} \cdot a_H)/(1 + K_{nj} \cdot a_H) \quad (23)$$

which is similar in form to Eq. 14 except that each statistical weight is modified by the terms under the multiplication sign. For each state i, the term under the multiplication sign runs over all protonizable groups j and is a function of the protonation constants K_{nj} K_{ij}, and K_{Nj}, and the hydrogen ion activity a_H. The population of each state is given by an equation similar to Eq. 12 and the average enthalpy function by Eq. 9. It must be noted that, in this case, the enthalpy of each state, ΔH_i, is given by:

$$\Delta H_i = \Delta H_i^o + \sum_{j}^{m} (F_{ij} \Delta H_{B,ij} - F_{nj} \Delta H_{B,nj}) \quad (24)$$

where H_{Bij} is the protonation enthalpy for site j in state i, and F_{ij} is its fractional degree of saturation [$F_{ij} = K_{ij} \cdot a_H/(1 + K_{ij} \cdot a_H)$].

The above equations permit a rigorous interpretation of the temperature and pH dependence of the heat capacity function. As an example, Fig. 8 illustrates the shape of the temperature-pH heat capacity surface calculated for apo-myoglobin. At pH values near neutral the thermal unfolding of apo-myoglobin conforms closely to a two-state transition. At lower pHs a partly folded intermediate becomes populated and the transition can be accounted for in terms of a three-state transition mechanism (Barrick and Baldwin, personal communication).

The experimental energetics for the overall folding/unfolding reaction of apo-myoglobin were measured calorimetrically by Griko et al. *(21)* and the energetic parameters for the intermediate were derived by Haynie and Freire *(24)*. The pKa values for the protonation of histidines in apomyoglobin were measured recently by NMR *(26)*. Four histidyl groups were found to have anomalously low pK_a values clustered around 5 (His 24, $pK_a < 4.8$; His 48, $pK_a = 5.2$; His 113, $pK_a < 5.5$; His 119, $pK_a = 5.3$). The titration of the histidines near to the heme binding site (His

64, His 93, and His 97) could not be observed. In the native state these histidyl residues are completely buried; in horse apo-Mb they do not titrate even at the lowest pH values that could be studied by NMR (pH 4.8). Since there are no buried carboxyl groups in the folded form of myoglobin and presumably also in apo-myoglobin, the low pH behavior appears to be attributable to the anomalous histidines.

As shown in Fig. 8, at pH values between 6 and 5 the heat capacity surface displays two well defined peaks corresponding to the heat and cold denaturation transitions. Under those conditions, the transition is experimentally close to a two-state transition. At pH values between 3 and 5, a significant intermediate population is found, especially at low temperatures, where it reaches about 100% of the molecules. The intermediate state denatures at constant temperature on lowering the pH below 3 or at constant pH on increasing the temperature. At pH values of 4 and lower, the heat capacity function does not exhibit a "measurable" peak *(see also* ref. *21)*.

The case of ribonuclease A highlights another aspect of 2D-DSC. The stability of ribonuclease A as a function of temperature and the concentration of cytidine-2'-monophosphate (2'CMP) has been recently studied by two-dimensional differential scanning calorimetry *(12)*. It was shown that this approach is able to resolve simultaneously the folding/unfolding and the binding energetics. Although the partition function in this case is similar to that in Eq. (23), it must be noted that in a calorimetric experiment the total ligand concentration, and not the ligand activity or free ligand concentration, is the quantity experimentally known. Therefore the partition function and all other thermodynamic functions must be recast in terms of the total ligand concentration. This is done by finding the zero of the equation:

$$[X]_{total} - [X]_{bound} - [X]_{free} = 0 \quad (25)$$

as discussed by Straume and Freire *(12)*. Figure 9 depicts the temperature-[2'CMP] heat capacity surface for ribonuclease A. Under all ligand concentration conditions the transition conforms to the two-state mechanism. The protein concentration used in the experiments performed to generate the surface was 0.219 m*M*. At zero ligand concentration the $\Delta H_{vh}/\Delta H$ ratio is equal to one. On introduction of the ligand, the $\Delta H_{vh}/\Delta H$ ratio at first is reduced substantially at partially saturating ligand concentrations (e.g., at 0.16 m*M* 2'CMP the $\Delta H_{vh}/\Delta H$ ratio is only 0.746)

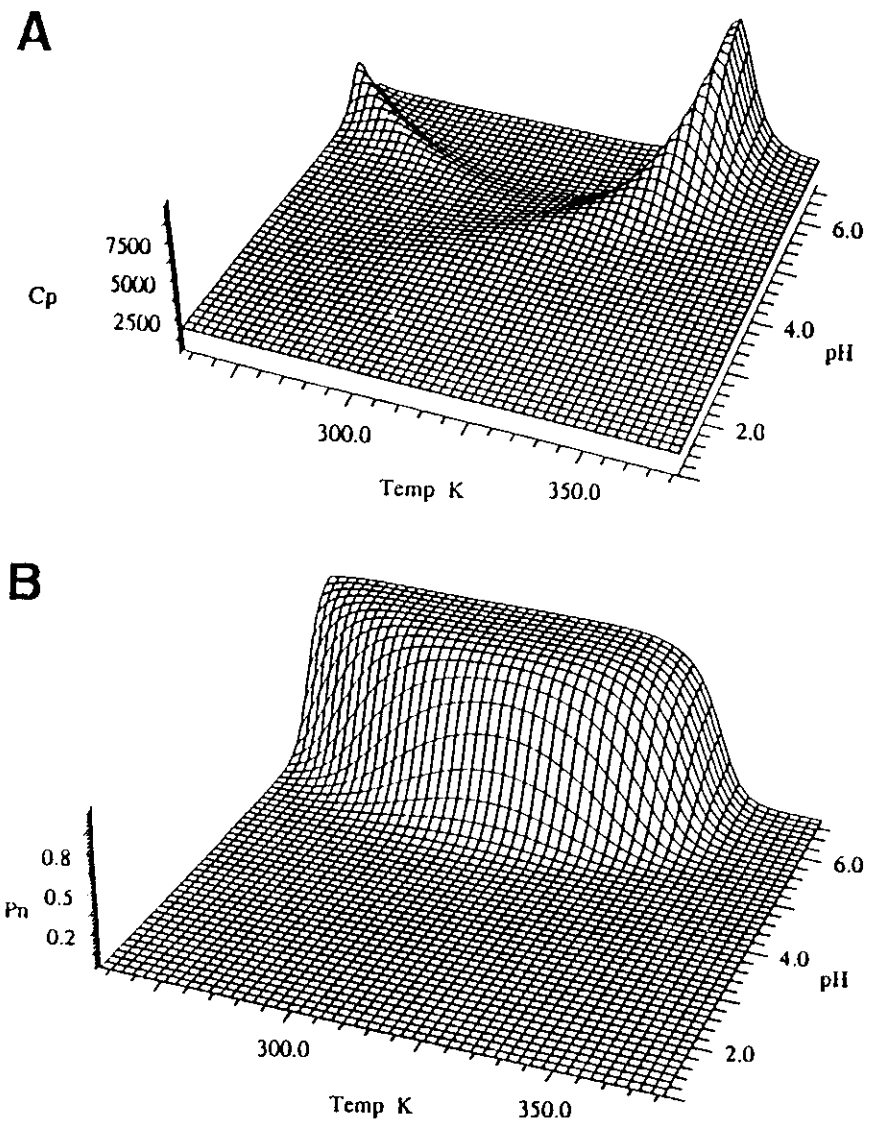

Fig. 8. Calculated heat capacity surface for apo-myoglobin as a function of temperature and pH (**A**) and population surfaces for the native (**B**), intermediate (**C**), and unfolded (**D**) states. The energetic parameter values used in the calculations were $\Delta H_I(25°C)$ = 8 kcal/mol, $\Delta C_{p,I}$ = 850 kcal/K/mol, $\Delta S_I(25°C)$ = 11.5 cal/K/mol; $\Delta H_U(25°C)$ = 28 kcal/mol, $\Delta C_{p,u}$ = 1550 cal · cal/K/mol, $\Delta S_u(25°C)$ = 63.5 cal/K/mol.

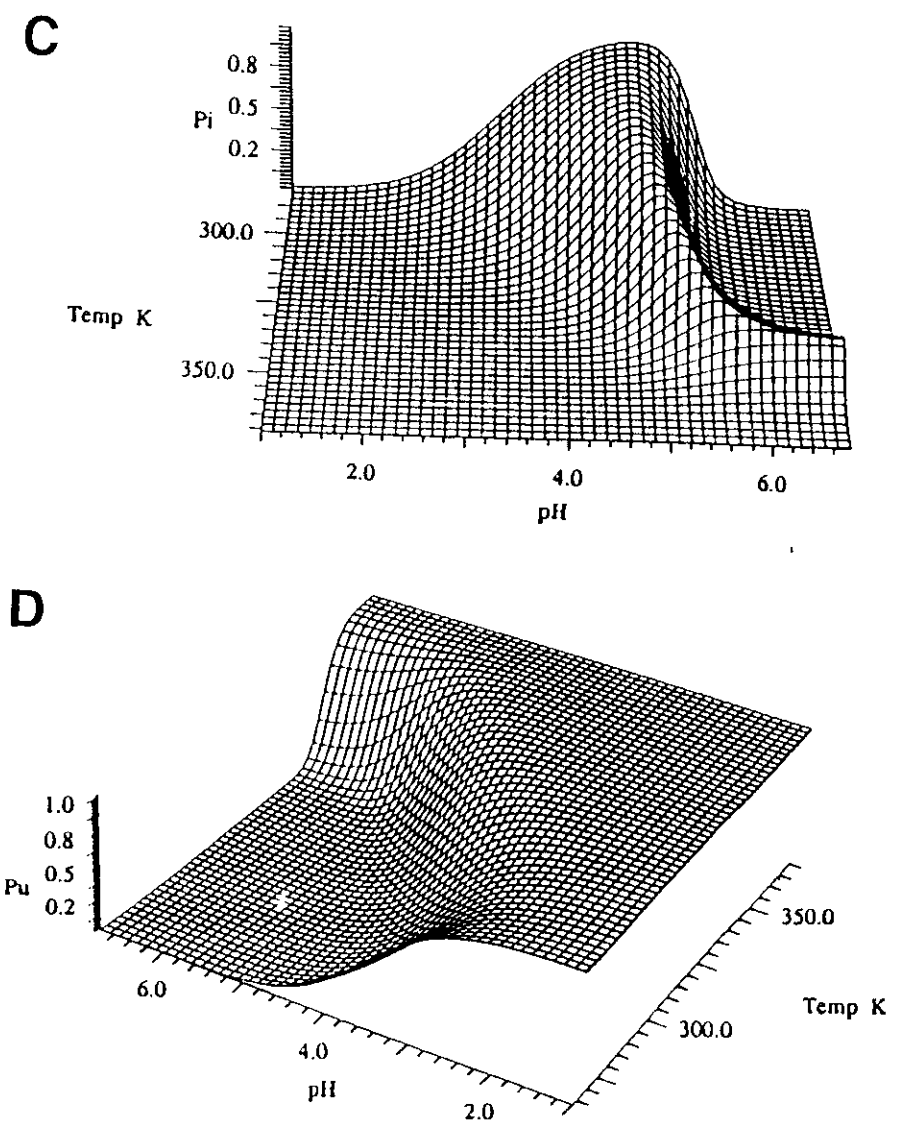

Fig. 8. *(continued)* For the simulation seven histidyl groups were assumed to have anomalous pK_as in the native state (4.5, 5.2, 5.2, 5.3, 2.5, 2.5, and 2.5). Two of the groups with pK_as around 2.5 were assumed to remain anomalous in the *I* state. The pK_as of the exposed histidyl groups were assumed to be 6 and the enthalpy of protonation of the histidyl residues –7 kcal/mol. Small variations in these values do not significantly affect the main features of the stability surfaces.

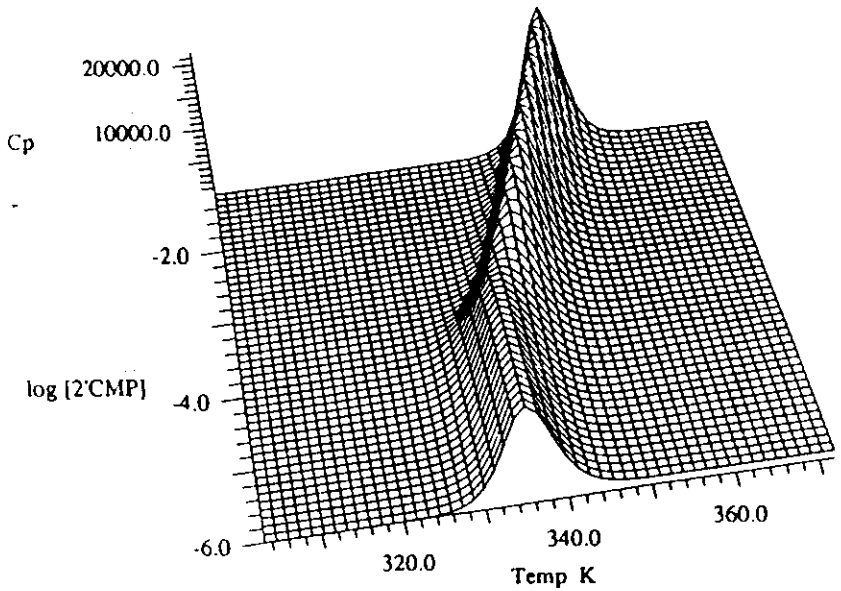

Fig. 9. Heat capacity surface as a function of temperature and 2'CMP for ribonuclease A. The surface was solved by Straume and Freire *(12)*, who obtained the following parameters by global nonlinear optimization of the experimental surface: ΔH = 109 kcal/mol, T_m^o = 61.9 °C, ΔC_p^o = 1.2 kcal/K/mo, ΔH_B = −18 kcal/mol, log K(25) = 6.19. It must be noted that at intermediate saturating conditions the $\Delta H_{vh}/\Delta H$ ratio for the individual peaks is significantly < 1 even though the transition is a two-state transition under all conditions (*see* ref. 1 for details).

after which it again returns to a value of one at saturating levels of 2'CMP. This behavior arises because, on increasing the temperature, the free 2'CMP concentration increases as a result of the reduced concentration of protein molecules in the native state. The remaining molecules in the native state are further stabilized by the additional free 2'CMP resulting in a broader transition profile. At fully saturating ligand concentrations, the $\Delta H_{vh}/\Delta H$ ratio again returns to one because the degree of ligand-induced structural stabilization no longer varies with the degree of completion of the reaction. The case of RNase A-2'CMP provides a vivid illustration that the $\Delta H_{vh}/\Delta H$ ratio can be different than one even for a two-state transition.

12. Structural Thermodynamics

The uniqueness of calorimetry is that it is the only technique that provides a direct experimental access to the overall thermodynamics and to the statistical thermodynamic partition function associated with a thermally induced transition. This experimental link to the most fundamental quantity in statistical thermodynamics has permitted the development of deconvolution procedures aimed at deducing the population and thermodynamics of the different states that become populated during the transition. Recently, a significant amount of research has been directed at developing a different type of experimental linkage: that between the partition function and the structure of a protein *(3,4,27–29)*.

In theory, the folding/unfolding partition function can be evaluated from structural information. Essentially, the strategy to calculate the folding/unfolding partition function starting from the molecular structure of the folded state involves generation of the set of most probable partly folded states using the crystallographic structure as a template and evaluation and assignment of the relative Gibbs free energies of those states. Once this task is accomplished, the evaluation of the partition function is straightforward by simple application of Eq. 14. Recently, an experimentally accurate structural parametrization of the folding/unfolding energetics of proteins has been developed (*see* refs. *3,4* and Chapter 1). This parametrization permits an evaluation of the relative probabilities of arbitrary partly folded states and especially those that can be generated using the crystallographic structure of the protein as a template *(24,27,29)*. This strategy allows determination of the set of most probable partly folded states of a protein. The initial results of this approach are encouraging.

It is expected that in the near future the combination of high resolution calorimetry, structural information, and the tools of structural thermodynamics should provide sufficient information for accurate predictions of protein stability and the effects caused by specific mutations, solvent composition, or other environmental variables.

Acknowledgments

This chapter was supported by grants from the National Institutes of Health (RR-04328, GM-37911, and NS-24520) and the National Science Foundation (MCB-9118687).

References

1. Privalov, P. L. and Khechinashvili, N. N. (1974) *J. Mol. Biol.* **86,** 665–684.
2. Privalov, P. L. and Makhatadze, G. I. (1990) *J. Mol. Biol.* **213,** 385–391.
3. Murphy, K. P. and Freire, E. (1992) *Adv. Protein Chem.* **43,** 313–361.
4. Murphy, K. P., Bhakuni, V., Xie, D., and Freire, E. (1992) *J. Mol. Biol.* **227,** 293–306.
5. Privalov, P. L. and Makhatadze, G. I. (1992) *J. Mol. Biol.* **224,** 715–723.
6. Griko, Y. V., Privalov, P. L., Sturtevant, J. M., and Venyaninov, S. Y. (1988) *Proc. Natl. Acad. Sci. USA* **85,** 3343–3347.
7. Privalov, P. L., Griko, Y. V., Venyaminov, S. Y., and Kutyshenko, V. P. (1986) *J. Mol. Biol.* **190,** 487–498.
8. Privalov, P. L. (1979) *Adv. Protein Chem.* **33,** 167–239.
9. Freire, E. (1989) *Comments Mol. Cell. Biophys.* **6,** 123–140.
10. Freire, E., van Osdol, W. W., Mayorga, O. L., and Sanchez-Ruiz, J. M. (1990) *Annu. Rev. Biophys. Biophys. Chem.* **19,** 159–188.
11. Freire, E. and Biltonen, R. L. (1978) *Biopolymers* **17,** 463–479.
12. Straume, M. and Freire, E. (1992) *Anal. Biochem.* **203,** 259–268.
13. Ramsay, G. and Freire, E. (1990) *Biochemistry* **29,** 8677–8683.
14. Shriver, J. W. and Kamath, U. (1990) *Biochemistry* **29,** 2556–2564.
15. Privalov, P. L. and Potekhin, S. A. (1986) *Methods Enzymol.* **131,** 4–51.
16. Rigell, C., de Saussure, C., and Freire, E. (1985) *Biochemistry* **24,** 5638–5646.
17. Montgomery, D., Jordan, R., McMacken, R., and Freire, E. (1993) *J. Mol. Biol.* **232,** 680–692.
18. Draper, N. and Smith, H. (1981) *Applied Regression Analysis,* Wiley, New York.
19. Johnson, M. L. (1983) *Biophys. J.* **44,** 101–106.
20. Johnson, M. L. and Frasier, S. G. (1985) *Methods Enzymol.* **117,** 301–342.
21. Griko, Y. V., Privalov, P. L., Venyaminov, S. Y., and Kutyshenko, V. P. (1988) *J. Mol. Biol.* **202,** 127–138.
22. Xie, D., Bhakuni, V., and Freire, E. (1991) *Biochemistry* **30,** 10,673–10,678.
23. Kuroda, Y., Kidokoro, S.-I., and Wada, A. (1992) *J. Mol. Biol.* **223,** 1139–1153.
24. Haynie, D. T. and Freire, E. (1993) *Proteins: Struct. Func. Genet.* **16,** 115–140.
25. Shrake, A. and Ross, P. D. (1990) *J. Biol. Chem.* **265,** 5055–5059.
26. Cocco, M. J., Kao, Y.-H., Phillips, A. T., and Lecomte, J. T. J. (1992) *Biochemistry* **31,** 6481–6491.
27. Freire, E. and Murphy, K. P. (1991) *J. Mol. Biol.* **222,** 687–698.
28. Freire, E., Murphy, K. P., Sanchez-Ruiz, J. M., Galisteo, M. L., and Privalov, P. L. (1992) *Biochemistry* **31,** 250–256.
29. Freire, E., Haynie, D. T., and Xie, D. (1993) *Prot. Structure Func. Genet.* **17,** 111–123.